University of Oxford



Moisture Generation and Transport at Ice Stream Margins

Submitted for the degree of MSc By Research

Author:
Alexander EW Győrffy

College:
St. Edmund Hall

ORA Submission Date August 31, 2016
Word Count 13,395

DECLARATION

During this research project I received a large amount of guidance from my supervisors: Prof. Ian Hewitt and Prof. Richard Katz. Both were regularly available to answer my queries and entertained much academic discussion, forming the basis of several key ideas propounded in this report. Their ongoing counsel and advice assisted me significantly throughout the project. The justifications, derivations, predictions, and final conclusions however, are my own, with many of the featured results found using my own scripts. I confirm that all formally presented material in the report is original unless explicitly stated otherwise.

I confirm that no parts of this thesis have already been accepted, or are being concurrently submitted for any degree, diploma, certificate or other qualification in this University or elsewhere.

ABSTRACT

Alterations to glacial mass balance brought about by dynamic changes in ice flow play a key role in the global climate system via sea-level rise, diminishing albedo and alterations to atmospheric circulation. A detailed understanding of these dynamics is therefore a prerequisite to making accurate predictions of future global ice extent and quantifying its feedbacks on the changing climate. Temperate zones are predicted to exist deep within the Antarctic ice sheet due to intense shear heating at ice stream margins. These are the lateral boundaries of fast-flowing regions known as ice streams: rivers of ice which may account for up to 90% of the flow into ice shelves and the surrounding oceans. Thus understanding how ice streams and their margins evolve under temperate ice-water dynamics is of great importance in the climate science community. However, current efforts to include meltwater in glaciological models do not fully couple the dynamic flows of ice and water necessary in describing the full physics in these temperate zones and hence the physics of ice stream margins.

We suggest using a two-phase fluid dynamical model to describe the movement of water through viscously deforming polycrystalline ice. We investigate the application of this theory to a planned experiment, designed to mimic glacial conditions and reproduce ice deformation in order to infer its rheology. Introducing the mathematics of two-phase flows, originally intended for applications in magma-mantle dynamics, we explain how these equations may equally be applied to ice-water mixtures. More specifically, we explain how they apply to an experimental setup, drawing inferences on the evolution of ice stream margins. Solutions are identified under constant stress boundary conditions, achieving a stable steady-state porosity φ of 2% assuming a viscosity constant λ much larger than that used from analogy with mantle rocks. That is, we predict that the viscosity of glacier ice is much more sensitive to changes in porosity than that of the mantle. Using this model, the total drainage from Dragon Margin of Whillans Ice Stream, in the Ross Ice Shelf, West Antarctica, due to englacial melting is 36 $\mathrm{m^3 yr^{-1}}$ per metre downstream. We also lay the groundwork for a two-phase 1D numerical model, and provide recommendations for further modelling and experimentation based on our results.

Contents

Chapter 1

Introduction

Alterations to glacial mass balance brought about by dynamic changes in ice flow play a key role in the global climate system via sea-level rise, diminishing albedo and alterations to atmospheric circulation. A detailed understanding of these dynamics is therefore a prerequisite to making accurate predictions of future global ice extent and quantifying its feedbacks on the changing climate.

Many ice masses, such as those that constitute mountain glaciers, are observed to be *polythermal*. That is, some parts of these glaciers are *cold*, sitting below the pressure-melting temperature, and some parts are *temperate*, sitting at the pressure-melting temperature, indicating the presence of small quantities of water. The existence of these temperate zones is well established in the mountainous alpine regions, as documented by Glasser (2011) for example, and pictured in Figure 1.1. However, advancing experimental and theoretical glaciology also implies the existence of temperate zones within the Greenland and Antarctic *ice sheets*, particularly in the vicinity of *ice stream margins* [Jacobson & Raymond (1998); Clarke et al. (2000); Schoof (2004, 2012); Beem at al. (2010); Perol & Rice (2011); Suckale et al. (2014)]. An *ice stream* is simply a region of an ice sheet that may move up to 2 or 3 orders of magnitude faster than the surrounding ice [Shabtaie & Bentley (1987)]. The ice stream margins then refer to the lateral boundaries of these ice streams, marking the interface between the narrow regions of fast-flowing ice and their relatively stagnant surroundings. Since average temperatures throughout the ice sheets are far below the pressure-melting point (with some regions reaching below $-30°$C), these temperate zones are predicted to be localised at the ice-bed interface, due to intense frictional shear heating within the margins.

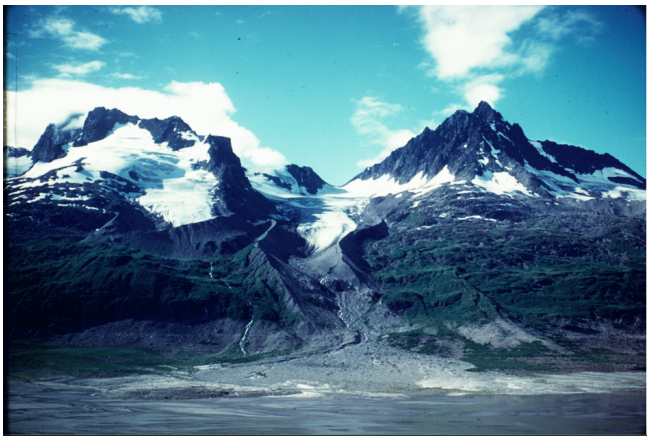


Figure 1.1: An image of an alpine polythermal glacier. http://climatehistories.innerasiaresearch.org.

Ice streams may account for up to 90% of the ice flux into the ice shelves and surrounding oceans in Antarctica [Bamber (2011); Rignot et al. (2011)] and a complete collapse of the

Antarctic ice sheet would raise the global sea level by 3-5 metres [Vaughan & Spouge (2002); Bamber et al. (2009)]. Thus understanding how ice streams and their margins evolve under temperate ice-water dynamics is of great importance in the climate science community. Some efforts to include melting in ice sheet models successfully describe the flow subglacially via an enthalpy conservation law [Aschwanden et al. (2012)], for example. Such models do not, however, fully describe englacial melt generation and transport, and do not fully couple the dynamics of ice and water necessary in describing the physics in these temperate regions, and hence the physics of ice stream margins.

In this report we suggest using a two-phase fluid dynamical model for temperate mixtures in order to describe the movement of water through viscously deforming polycrystalline ice. In addition to this, we investigate the application of this two-phase theory to a planned experiment, using similar apparatus to that used by Iverson & Peterson (2011), which has been designed to mimic glacial conditions and reproduce ice deformation in order to infer its texture and rheology. The experiment consists of an annular aluminium chamber which holds a ring of ice-water mixture maintained at the pressure-melting temperature in a sealed room. Vertical and horizontal stresses are applied to the temperate ice, and water is drained through a permeable interface at the base of the chamber reproducing the effects of compaction, drainage and shear dissipation.

Commencing with a brief introduction to glaciology and ice dynamics, we will go on to review the current literature and discuss the mathematics and physics of two-phase flows as laid out by McKenzie (1984), originally intended for applications in magma-mantle dynamics. We will then explain how these equations may equally be applied to ice-water mixtures and more specifically, to our experimental setup in order to draw inferences on both temperate ice dynamics and the evolution of ice stream margins. We will then work through to derive analytical solutions in a few simplified cases before laying the groundwork for a 1D numerical model, which may be used in order to derive a more complete solution. Finally, we provide some results and predictions, as well as recommendations for further modelling and experimentation based on these findings, and discuss some potential research ideas for the future.

Chapter 2

Background

Below, I give a brief introduction to ice dynamics; for a more thorough and in-depth coverage of the topic, see *The Physics of Glaciers* by Cuffey & Paterson (2010). §2.1 provides an intentionally "maths free" introduction, with Chapter 3 summarising the accompanying equations.

2.1 Ice Sheets & Ice Stream Dynamics

A glacier may be thought of as a large slow flowing river of ice, draining areas in which snow accumulates, much as a river drains catchment areas where rain falls [Fowler (2013)]. In fact, glacier flow may be described by very similar physics to river flow. Although glacier ice is of course solid, it may deform by the gradual creep of dislocations within its crystal lattice, which cumulatively forms the fabric of the ice, and in this way, the ice effectively behaves like an enormously viscous fluid. As a result, the rate of glacier flow is much lower than that of water, and indeed we observe velocities ranging from 10s to 100s of metres per year. Typical glaciers are hundreds of metres in depth, kilometres in width and tens of kilometres in length.

Glaciers are often compared to rivers since their flow is usually channelised, but it isn't always this simple. Sufficiently extended ice masses with a base resting on solid land are referred to as *ice sheets*. The way these masses flow is quite different, their viscous deformation properties more akin to droplet-like behaviour. Large land masses with polar climates accumulate snow in regions of higher altitude, which compresses to form firn, then compresses further to form ice. The ice then flows outward, much as a drop of treacle on a table will flow as a viscous gravity current. Equilibrium can be maintained through a balance between accumulation in the centre and ablation at the margins. This typically occurs through a combination of melting of the ice in the warmer climate at the ice sheet margins, or more likely, through the dynamic process of iceberg calving.

Earth has two major ice sheets, namely those in Antarctica and Greenland. These sheets are thousands of kilometres in extent, and several kilometres deep. Since the ratio of extent to depth, or *aspect ratio*, is so large, it is relatively straightforward to mathematically model these ice masses using the so called *shallow-ice approximation*, as is routinely done by glaciologists. Ice sheets do not tend to drain uniformly to their margins from their central accumulation zones, rather the outflows from their catchment areas are concentrated into fast-moving streams. Of

all the phenomena associated with ice sheets, it is these *ice streams* that are arguably of most interest and most critical environmental importance. These are localised narrow bands of fast-moving ice, often flowing at a rate of several metres per day. They are typically kilometres in depth, tens of kilometres in width and hundreds of kilometres in length.

Increasing average temperatures in our atmosphere and oceans are leading to a more rapid melting of the ice sheets, though much greater danger lies in the ice's dynamical response to warming and melting [Schoof & Hewitt (2013)]. Ice streams are the dominant negative component in this mass balance, accounting for up to 90% of the Antarctic ice flux into ice shelves and ultimately into the oceans [Bamber (2011); Rignot et al. (2011)]. These streams are separated by ridges of stagnant ice which flow up to 2 to 3 orders of magnitude slower than the ice stream, with large strain rates leading to deformation and recrystallisation, softening the ice, and forming crevasses at their lateral boundaries, or *shear margins*. Some particularly chaotic crevassing due to localised intense shear straining at the surface of Whillans ice stream is shown reflecting white in Figure 2.1 where the position of Dragon Margin has also been identified. The position of Whillans ice stream in the Ross Ice Shelf is then shown in Figure 2.2. Despite their clear importance, our understanding of ice stream margin dynamics remains incomplete; the theory is yet to be thoroughly investigated.

Ice streams increase their flow speed by carving out deep channels through which they flow. This produces a clear positive feedback loop since the deeper the ice flow, the larger the corresponding basal stress, and the warmer the basal ice will become due to the increasing production of frictional heat. This in turn increases the melt rate and speeds up the ice flow. These effects act to strengthen the flow and increase mass loss from the ice sheet.

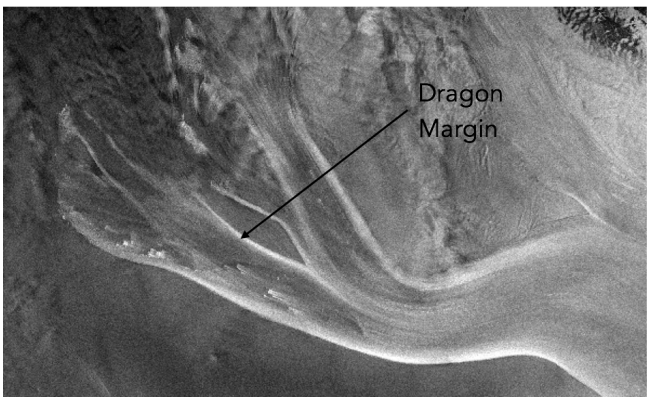


Figure 2.1: Whillans Ice Stream, www.earthzine.org.

The reason for the existence of some modern ice streams has been investigated since pre-existing topographic constraints may have caused ice to be channelised into bedrock troughs [Stokes & Clark (2001); Vaughan et al. (2006)]. In spite of these positive results, in many other cases there seem to be no obvious topographic controls on the flow [Cuffey & Paterson (1969); Shabtaie & Bentley (1987)]. Contrary to the outlet glaciers which flow through mountain gaps and are thus confined by the shape of the land surface, topography cannot fully explain the location of the fast-flowing ice streams in the Ross Ice Shelf, West Antarctica [Shabtaie & Bentley (1988)], for example. Further evidence that ice-stream width is not controlled by topography alone comes from evidence that some margins have shifted in the past [Jacobel et al. (1996, 2000); Clarke et al. (2000); Fahnestock et al. (2000)] or are currently migrating [Bindschadler & Vornberger (1998); Harrison et al. (1998); Echelmeyer & Harrison (1999)]. And so there still remains considerable uncertainty in establishing the fundamental controls on these dynamics.

A range of observations associates the presence of ice streams with subglacial meltwater. Although it is known to reduce resistance to ice flow, water production is itself a consequence of viscous and frictional dissipation by the ice, introducing complex feedbacks into the system which, at present, are poorly understood. Fast ice flow is hypothesised to be primarily controlled by the presence and time variability of pressurised water at the base [Schoof (2010)], and this basal water can be transported laterally and is able to refreeze at significant rates, especially over highly variable bed topography [Bell et al. (2011)]. Research on the evolution of paleo-ice streams by Stokes & Clark (2001) also highlights the important role these feedbacks have played in previous ice sheet collapse but, crucially, current ice-sheet models are incapable of correctly resolving them.

Since ice streams have been observed to periodically turn on and off, Christoffersen (2003) provided a quantitative explanation for the "turning off" of ice streams observed in West Antarctica, showing that a reduction in till porosity of just a few percent is sufficient to impede fast flow, shutting down these streams after less than 100 years of basal freezing. In turn, Kyrke-Smith et al. (2014) investigated the "turning on" of ice streams by using a hydrological model in which the subglacial flow was fed by basal melting. Using this model, the distributed film and ice sheet remain stable for a sufficiently small amount of meltwater production, but for larger amounts the ice-water system tends to become unstable, and ice streams form spontaneously as a consequence.

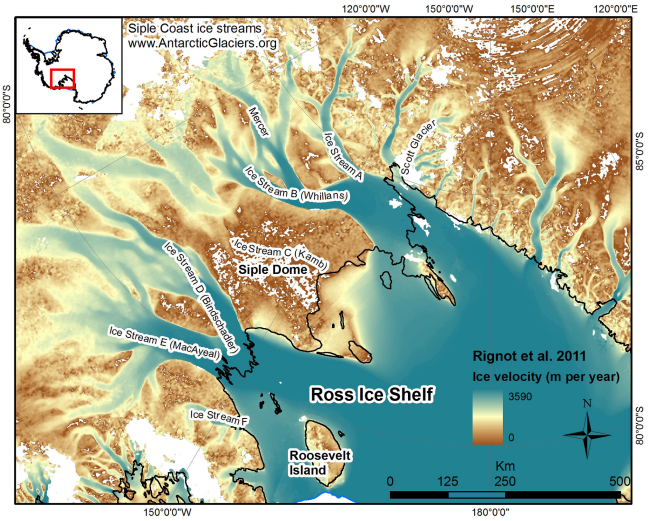


Figure 2.2: Whillans Ice Stream within the Ross Ice Shelf, http://cdn.antarcticglaciers.org.

As we expect an increase in water production to result in an increase in water pressure, assuming Darcian flow, such high pressures would also decrease till viscosity, enhancing the ice flow. Price (2008) investigated inland ice stream migration, suggesting that basal meltwater production and basal sliding causes the sliding transition to migrate upstream over time, enhancing the flow further. It has since been suggested, by Schoof (2012) and others, however, that potential instabilities of this kind may be prevented by the influx of colder ice into the stream, though this is simply a working theory. In general, what might be most important in controlling the migration of ice stream margins is still largely debated.

Bougamont et al. (2011) argue that the dynamic response of the Greenland Ice Sheet depends on feedbacks between surface meltwater delivery to the subglacial environment and ice flow. They found that the weakening and strengthening of subglacial sediment, associated with the seasonal delivery of surface meltwater to the bed, modulates ice flow consistent with observations. They also proposed that sedimentary control on ice flow is a viable alternative to models which use evolving hydrological systems, suggesting meltwater may not be crucial in

understanding dynamics at the bed.

The role of englacial meltwater, that is, the role of water within the ice itself, in facilitating ice flow has also been recognised with available experimental evidence suggesting that an increase in liquid water fraction from 0 to 1% softens temperate ice by a factor of 3 [Duval (1977); Lliboutry & Duval (1985)]. Advancing research [Jacobson & Raymond (1998); Clarke et al. (2000); Schoof (2004, 2012); Beem at al. (2010); Perol & Rice (2011); Suckale et al. (2014)] also implies the existence of temperate zones, that is, regions of ice sustained at the pressure-melting temperature, within the Greenland and Antarctic ice sheets, particularly in the vicinity of ice stream margins.

Cold-ice models are those that assume all ice to be characterised by a temperature below the pressure-melting point and describe the entire ice mass as an incompressible, viscous and heat-conducting single component fluid. Earth's ice sheets are known to consist mainly of this type of ice [Greve (1997)], and meltwater feedback mechanisms may still be seen in *cold-ice* models [Payne et al. (2000)], though such mechanisms will significantly increase in strength when tracking liquid water fraction i.e. when the melting process is included.

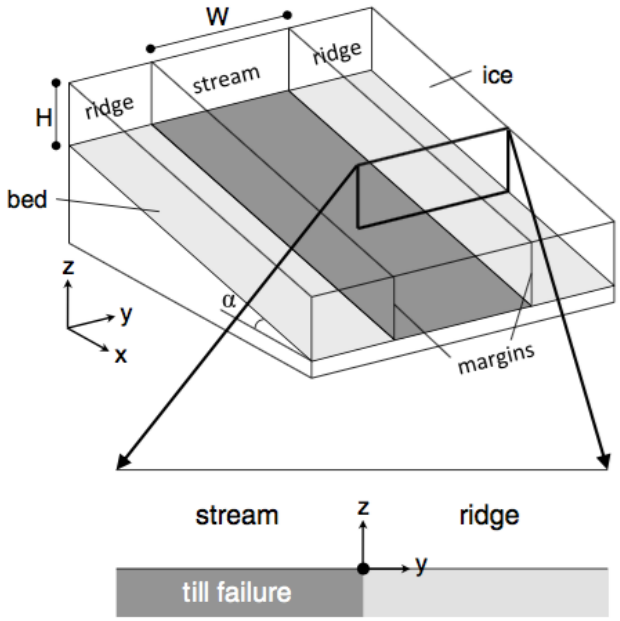


Figure 2.3: Ice stream margin model [Suckale et al. (2014)].

Water generation within temperate ice is primarily down to dissipative heating. For this reason, *polythermal* models, that is, models that define distinct cold and temperate regions, are able to compute a more physical basal melt rate. Cold-ice methods, however, must model dissipative heating in temperate ice by either instantaneously transporting the energy to the base or immediately and unphysically losing that energy. Transport within a polythermal model avoids such an issue by advecting the generated liquid water downstream, increasing the downstream basal melt rate caused by englacial drainage in a physical way. Thus the more complete energy conservation achieved by a polythermal model improves the modelled distribution of basal melt both spatially and temporally. Enthalpy methods used in metallurgy and magma-mantle dynamics [Katz (2008)] have now been adapted to describe polythermal glacier flow by Aschwanden et al. (2012), possessing this distinct advantage.

Though difficult to observe directly, there is good reason to believe that a polythermal model is more physically accurate than a cold-ice model within the vicinity of ice stream margins. Clarke et al. (2000) conducted a radar survey at Dragon Margin finding diffractors in the ice sheet existing over 230m above the bed and interpreting them as temperate ice. They note that a Caltech group had drilled deep into the ice at Dragon Margin, reporting that at approximately

50m above the bed, the drill began encountering abnormal resistance within layers that were strongly suggestive of morainal debris. One of the possible mechanisms for the formation of this debris is from meltwater processes depositing sediment over long periods of time, indicating that the morainal debris is a result of the presence of englacial water or perhaps even channel development at the bed.

This idea is also supported theoretically by Suckale et al. (2014) who explored the conditions under which intense shearing in ice stream margins, here defined as the interface between the ice stream and its neighbouring ice ridge, may lead to deformation-induced melting. They proposed using a 2D cold-ice model that represents a cross section through the ice stream margin perpendicular to the downstream flow direction, as shown in Figure 2.3. The model assumes that the ice flow is driven by a relatively small gravitational driving stress that is equilibrated primarily through basal drag and laterally shear stressed zones at the margins [Whillans and van der Ween (1993)], where side drag provides most of the resistance to the driving stress [Joughin et al. (2004)]. Limiting the temperature to the pressure-melting point so as to estimate melt rates based on latent heat, they too focussed on Dragon Margin of Whillans Ice Stream. In doing this they showed that a close match to the downstream surface velocity profile provided by Echelmeyer et al. (1994) could be achieved only in simulations which developed a large temperate zone within the margin.

Perol & Rice (2015) and Perol et al. (2015) took this idea further, suggesting that in some cases, such a large amount of melt is generated due to frictional heating that it accumulates, advecting downstream into a Röthlisberger channel at the base of the margin. In such a case the shear margin is controlled by the presence of this drainage channel. Their hypothesis is supported by the observation of a cavity filled with flowing water between the base of the ice sheet and the bed at the margin of Kamb ice stream [Vogel et al. (2005)].

The motivation for using a two-phase fluid dynamical framework for coupled ice-water flow arises from the lack of self-consistency of current modelling efforts, in spite of their successes. These models still do not fully account for phase transitions and their dynamical feedbacks both within and below regions of temperate ice. Energy, mass and momentum conservation follow naturally from two-phase fluid dynamics with melting and re-freezing encapsulated by the coupled equations. This type of thinking is not entirely new, however, since Hutter (1982) introduced a mathematical model of the flow and temperature distribution of polythermal glaciers, which regarded temperate ice as a binary mixture of ice and water. Fowler (1984) also described ice-water interactions by making an analogy with the flow through the veins of a porous medium [Nye & Frank (1973)], and utilising Darcy's law, the second momentum equation of a two-phase flow model with porous geometry. We now wish to develop these simpler models by deriving a full two-phase fluid dynamical theory in §§2.2-3.1

2.2 McKenzie's Two-Phase Equations

The two-phase fluid dynamical theory of coupled magma-mantle dynamics was first derived by McKenzie in 1984, motivated by the insufficient predictive capabilities of the equations of mantle convection. The goal was to derive a set of equations which included magmatism,

and hence reproduced a range of magmatic observations (volcanism, for example) that would reduce to basic mantle convection in the limit of zero melting. Over time these equations were modified and further generalised by Katz (2015) and others, aiming to provide insight into the mechanics, energetics and magma petrology, predicting behaviour that hadn't been captured by the equations of mantle convection.

The equations of single-phase viscous mantle convection are well known, and follow what is known as a *Stokes regime*, where viscous forces dominate over inertial forces.

$$\nabla \cdot \mathbf{v} = 0, \tag{2.1}$$

$$0 = -\nabla p + \nabla \cdot \boldsymbol{\tau} + \rho \mathbf{g}, \tag{2.2}$$

$$\rho c_p \left(\frac{\partial T}{\partial t} + \mathbf{v} \cdot \nabla T \right) = k \nabla^2 T + \rho \mathcal{H}. \tag{2.3}$$

Here $\mathbf{v}$ is the mantle velocity, p is the mantle pressure, $\boldsymbol{\tau}$ is the deviatoric stress tensor, ρ is the mantle density, $\mathbf{g} = g\hat{\mathbf{k}}$ is the gravity vector, c_p is the specific heat capacity, T is the temperature, k is the thermal conductivity and $\mathcal{H}$ is the rate of heat production per unit mass. Equation (**??**) is a statement of mass conservation, approximating the mantle as incompressible. Equation (**??**) is a statement of momentum conservation, showing that gravity is balanced by pressure gradients and deviatoric stresses within the mantle. Equation (**??**) is a statement of energy conservation. Note the $+\rho\mathcal{H}$ term, which represents additional heat input/output. This is an important contribution to conservation of energy for many different physical systems, and we will expand upon these forms of heat as we go on.

The most crucial shortcoming of equations (**??**)-(**??**) is that they do not take into account the presence of magma, the liquid contribution to the dynamics. McKenzie suggested tracking this contribution using a quantity that characterises the ratio of magma to mantle content within the mixture, and who's spatial and temporal variation would provide key information about the system's compaction and drainage. This quantity is known as the liquid volume fraction, or *porosity*. In order to define the porosity with sufficient generality for this report we borrow the notion of a representative volume element or RVE from Katz (2015). Since we intend to average physical properties over this element, we require that the RVE contains a sufficient number of mantle grains such that this average is indeed "representative" i.e. not dependent on the specific details of which grains happen to be within it.

Defining an indicator function $\mathcal{Q}(\mathbf{x})$, we identify the solid (mantle) and the liquid (magma) components within the RVE

$$\mathcal{Q}(\mathbf{x}) = \begin{cases} 1 & \text{if there is magma at } \mathbf{x}, \\ 0 & \text{if there is mantle at } \mathbf{x}. \end{cases} \tag{2.4}$$

The indicator function simply tells us which phase is present at any given point $\mathbf{x}$. More importantly, it allows us to define the porosity φ as the volume fraction of the liquid phase within the RVE

$$\varphi = \frac{1}{V} \int_{RVE} \mathcal{Q}(\mathbf{x}) dV, \tag{2.5}$$

where the integral runs over all $\mathbf{x} \in \text{RVE}$, and V is the total volume. Some modern adaptations of two-phase flows account for many different thermodynamic components, including multiple materials e.g. olivine, peridotite etc., but here we just consider one material type, and therefore the volume fraction of the solid phase must be equal to $1 - \varphi$.

We will now refer to the liquid "mass" as $\rho_f \varphi$ and the solid "mass" as $\rho_m(1-\varphi)$. Defining these quantities allows us to utilise the same conservation principles as we would use in single-phase fluid dynamics in order to derive the governing equations of two-phase flows. Omitting full derivations we have

$$\Gamma = \frac{\partial \rho_f \varphi}{\partial t} + \nabla \cdot (\rho_f \varphi \mathbf{v}_f), \tag{2.6}$$

$$-\Gamma = \frac{\partial \rho_m (1-\varphi)}{\partial t} + \nabla \cdot (\rho_m (1-\varphi) \mathbf{v}_m), \tag{2.7}$$

$$\nabla P_f = \nabla \cdot \eta (\nabla \mathbf{v}_m + (\nabla \mathbf{v}_m)^T) + \nabla \left[\left(\zeta - \frac{2\eta}{3} \right) \nabla \cdot \mathbf{v}_m \right] + \rho \mathbf{g}, \tag{2.8}$$

$$\varphi(\mathbf{v}_f - \mathbf{v}_m) = -\frac{K}{\mu} \nabla (P_f + \rho_f g z). \tag{2.9}$$

i subscripts denote quantities corresponding to the i^{th} phase with subscripts f describing those in the fluid phase and m the solid matrix phase with $\rho = \rho_m - \rho_f$. We also have Γ, the melt rate, K, the permeability of the solid matrix, μ the dynamic viscosity of magma, ζ the bulk viscosity and η the effective shear viscosity.

Equations (**??**) and (**??**) are statements of mass conservation for the fluid and matrix phases respectively. Equation (**??**) is a statement of momentum conservation for the bulk aggregate and (**??**) a statement of momentum conservation for the fluid, recognisable as a two-phase version of Darcy's law. It will also be useful to derive a conservation of mass equation for the solid-liquid aggregate. Taking each phase density to be constant (an assumption known as the Boussinesq approximation), dividing equations (**??**) and (**??**) through by ρ_i and adding them together gives

$$\nabla \cdot (\varphi \mathbf{v}_f + (1-\varphi)\mathbf{v}_m) = \frac{\rho}{\rho_m \rho_f} \Gamma. \tag{2.10}$$

The term on the right hand side is usually neglected since $\rho_m \rho_f \gg \rho$. This is then known as the *extended* Boussinesq approximation. It is these equations (**??**)-(**??**) or often a subset of these equations, which are usually referred to as the *McKenzie equations*. Upon inspection we can readily see that having a non-zero melt rate $\Gamma \neq 0$ allows the porosity φ to evolve non-trivially over time by phase change [equations (**??**) & (**??**)] as well as via segregation of one phase from the domain [equation (**??**)].

While the equations of single-phase mantle convection provide us with a single statement of conservation of mass, the McKenzie equations provide us with two coupled statements, one for each phase. The same is true for momentum conservation. Note that in (**??**) we have expanded out what would be the divergence of the mantle stress tensor into two terms: $\nabla \cdot \eta (\nabla \mathbf{v}_m + (\nabla \mathbf{v_m})^T)$, representing the shear stresses and $\nabla \left[\left(\zeta - \frac{2\eta}{3} \right) \nabla \cdot \mathbf{v}_m \right]$, a combination

of compressible deviatoric and normal stresses. The stress tensor σ_{ij} is simply a sum of all the deviatoric stresses τ_{ij} and the isotropic stresses $-p\delta_{ij}$, where δ_{ij} is the *Kronecker-δ* symbol, sometimes referred to as the *identity tensor*.

These two mantle stress terms are derived from the full form of the bulk stress tensor $\boldsymbol{\sigma} = \varphi\boldsymbol{\sigma}_f + (1-\varphi)\boldsymbol{\sigma}_m$ where the subscripts again refer to each individual phase's stress tensor. In continuum mechanics, the stress tensor is most generally given in the form

$$\sigma_{ij} = -p\delta_{ij} + \zeta\delta_{ij}\partial_k v_k + \mu(\partial_j v_i + \partial_i v_j - \frac{2}{3}\delta_{ij})\partial_k v_k. \tag{2.11}$$

where we have implicitly employed the Einstein summation convention. Taking the magma viscosity μ to be much smaller than the mantle viscosity η, along with $\varphi \ll 1$, we use the approximation $\boldsymbol{\sigma} \approx \boldsymbol{\sigma}_m$. Equation (**??**) is then the vectorised version of (**??**).

In order to complete this system of equations, we need a statement of two-phase energy conservation. Before going on to write down this statement, we should revisit single-phase energy conservation (**??**) in a more general form. This form is sometimes referred to as an *advection-diffusion-reaction* equation

$$\frac{\partial T}{\partial t} = \nabla \cdot (D\nabla T) - \nabla \cdot (\mathbf{v}T) + R, \tag{2.12}$$

where D is the diffusivity coefficient and R is a quantity describing the sources and sinks of the system. Note that for mantle convection (and for convection equations more generally) we have $D = k/\rho c_p$ and $R = \mathcal{H}/c_p$. The three terms on the right hand side of (**??**) each play a crucial role in governing the system's temperature evolution. $\nabla \cdot (D\nabla T)$ represents the diffusion of heat within the fluid, $\nabla \cdot (\mathbf{v}T)$ describes the advection of heat for an incompressible fluid and R includes contributions such as radiative heating and viscous dissipation. It's important to note that the advection-diffusion-reaction equation could hold for any conserved variable of interest. That is, T could in fact be replaced in this equation by any conserved variable evolving by advection, diffusion or otherwise.

As expected, the new statement of energy conservation for a two-phase system is a little more complex than its single-phase equivalent. Using our definitions of the liquid and solid masses as $\varphi\rho_f$ and $(1-\varphi)\rho_m$, we construct a similar equation, adapted from Rudge et al. (2011):

$$\varphi\rho_f \frac{D_f U_f}{Dt} + (1-\varphi)\rho_m \frac{D_m U_m}{Dt} = \Gamma\Delta U + \mathfrak{R}. \tag{2.13}$$

Here $D_i/Dt = \partial_i/\partial t + \mathbf{v} \cdot \nabla$ and U_i are the Lagrangian derivative and the internal energy per unit mass for the i^{th} phase respectively, and $\mathfrak{R}$ is given most generally by

$$\mathfrak{R} = Q - \nabla \cdot \mathbf{q} - P\nabla \cdot \bar{\mathbf{v}} + \Psi. \tag{2.14}$$

Q is the rate of internal heat production, $\mathbf{q}$ is the diffusive heat flux and $\bar{\mathbf{v}} = \varphi\mathbf{v}_f + (1-\varphi)\mathbf{v}_m$ is the mean velocity of the magma-mantle mixture. Ψ represents viscous dissipation within the aggregate, and is written as

$$\Psi = \frac{\mu\varphi^2}{K}(\mathbf{v}_f - \mathbf{v}_m)^2 + \zeta(\nabla \cdot \mathbf{v}_m)^2 + \frac{\eta}{2}\left(\nabla\mathbf{v}_m + (\nabla\mathbf{v}_m)^T - \frac{2}{3}\mathbb{I}(\nabla \cdot \mathbf{v}_m)\right)^2. \tag{2.15}$$

Here $\mathbb{I}$ denotes the identity tensor in matrix notation. The first term on the right hand side of (**??**) represents magma-mantle segregation, the second term represents matrix compaction and the third term represents stresses in the solid-liquid aggregate. Note that the first term is only well-defined for multi-phase flows and the second term is equal to zero for an incompressible single-phase flow. It is clear from this equation that viscous dissipation plays a much more complex and important role in two-phase flows than it does in the equations of mantle convection, a key additional feature in investigating the role of magma in the mantle matrix.

Chapter 3

A Model for Temperate Ice-Water Flow

In §2.1 the basics of modelling ice dynamics and relevant literature were discussed, introducing some of the ways in which mathematical geoscientists are attempting to solve the current problems of interest in the field. We then moved on to introduce the McKenzie equations for coupled magma-mantle dynamics in §2.2, which self-consistently take account of the presence of magma: accounting for many earth observations for which the equations of mantle convection could not. In this chapter, we wish to use the McKenzie equations as a guide to derive a similar model for temperate ice.

Typical methods used by glaciologists to model viscous ice flow describe the dynamics using a single-phase Stokes regime in which the presence of meltwater is either ignored, or is included in the model in a way in which it is effectively decoupled from the ice. The basic equations of Stokes flow are those of mass and momentum conservation, which for an incompressible flow with constant ice density are

$$\nabla \cdot \mathbf{u} = 0, \tag{3.1}$$

$$0 = -\nabla p + \nabla \cdot \boldsymbol{\tau} + \rho \mathbf{g}. \tag{3.2}$$

Here $\mathbf{u}$ is the ice velocity, $\mathbf{g}$ is the gravity vector, p is the ice pressure and ρ, the ice density. These conservation principles are supplemented by the energy equation, which can be written in the form

$$\rho c_p \left(\frac{\partial T}{\partial t} + \mathbf{u} \cdot \nabla T \right) = k \nabla^2 T + \tau_{ij} \dot{\epsilon}_{ij}, \tag{3.3}$$

where we have employed the summation convention in the last term ($A_{ij}B_{ij} = \Sigma_{ij} A_{ij} B_{ij}$). In comparing equation (**??**) to equation (**??**), the mantle convection heating term $+\rho\mathcal{H}$ has now been replaced with the term $\tau_{ij}\dot{\epsilon}_{ij}$, where $\dot{\epsilon}_{ij} = 1/2(\partial_i u_j + \partial_j u_i)$ denotes the strain-rate tensor. This term represents viscous dissipation within the ice matrix. Employing the standard relationship between stress and strain for a viscous incompressible fluid $\tau_{ij} = 2\eta\dot{\epsilon}_{ij}$, we utilise the most popular choice of flow law for ice, commonly known as Glen's law

$$\dot{\epsilon}_{ij} = \mathcal{A}(T)\tau^{n-1}\tau_{ij} \tag{3.4}$$

to determine $\eta(T, \tau)$. Here the second stress invariant is given by $2\tau^2 = \tau_{ij}\tau_{ij}$ and $\mathcal{A}(T)$ is a temperature dependent rate factor, and so we can identify the effective viscosity as

$$\eta = \frac{\tau^{1-n}}{2\mathcal{A}}. \tag{3.5}$$

These are the single-phase equations most often used to model dynamic behaviour throughout the bulk of a cold ice sheet or glacier. In the same way that mantle convection fails to account for the effects of magmatism, these equations fail to account for the effects of meltwater in temperate ice. This failure cannot be entirely reconciled by including water in the model in some way so that it simply coexists with the ice. In order to construct a fully self-consistent model, we should also take into account the transfer of mass from the solid phase to the liquid phase, and its dynamical effects on the aggregate.

In §2.2 the equations for two-phase mass and momentum conservation were shown to be

$$\Gamma = \frac{\partial \rho_f \varphi}{\partial t} + \nabla \cdot (\rho_f \varphi \mathbf{v}_f), \tag{3.6}$$

$$-\Gamma = \frac{\partial \rho_m (1-\varphi)}{\partial t} + \nabla \cdot (\rho_m (1-\varphi) \mathbf{v}_m), \tag{3.7}$$

$$\nabla P_f = \nabla \cdot \eta(\nabla \mathbf{v}_m + (\nabla \mathbf{v}_m)^T) + \nabla \left[\left(\zeta - \frac{2\eta}{3} \right) \nabla \cdot \mathbf{v}_m \right] + \rho \mathbf{g}, \tag{3.8}$$

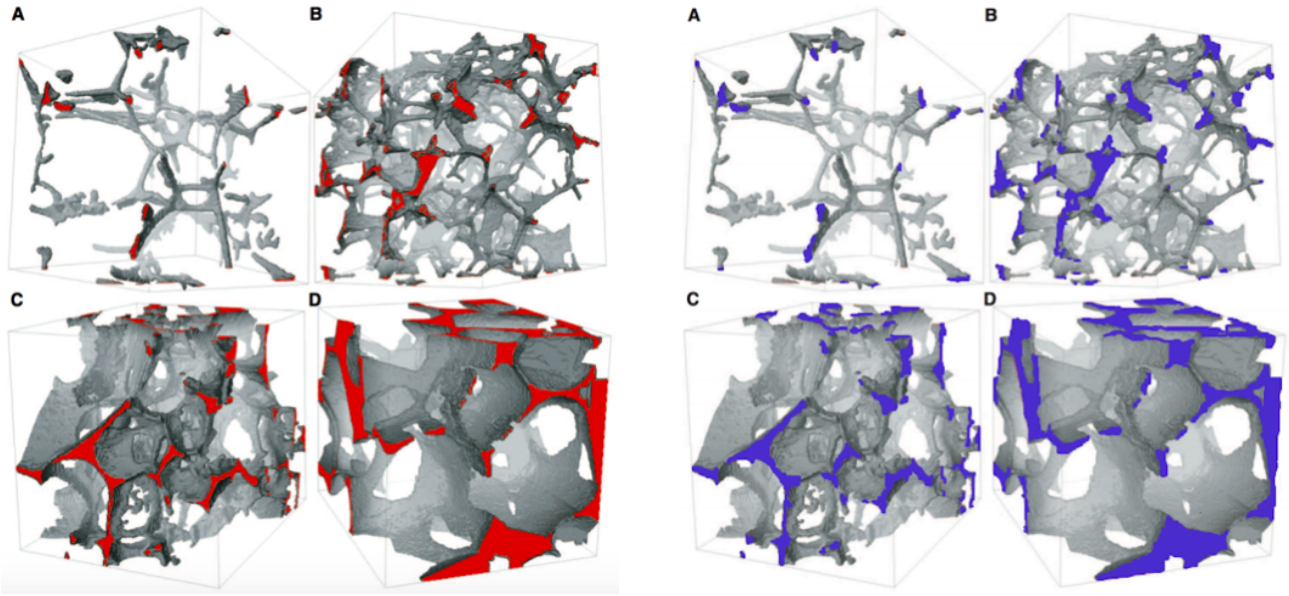
$$\varphi(\mathbf{v}_f - \mathbf{v}_m) = -\frac{K}{\mu} \nabla (P_f + \rho_f g z). \tag{3.9}$$

Since we have discussed some evidence suggesting that the presence of ice stream margins can be strongly associated with the existence of temperate zones, we recommend using a two-phase fluid dynamical model to describe meltwater flowing through temperate ice. Furthermore, since both magma-mantle mixtures and ice-water mixtures are simply aggregates of crystals with interstitial melt, we might expect coupled ice-water dynamics should be well approximated by the McKenzie equations (**??**)-(**??**) within these temperate zones: see Figure 3.1. In comparing these two mixtures, we will have to take care when deciding which simplifications can be made to the McKenzie equations in this new context. Identifying the dominant processes, and thus which terms in the equations can be considered negligible in each of these areas of earth sciences produces quite different results. Modelling a large ice mass as a cold and highly viscous incompressible single-phase fluid is quite reasonable for the most part, and so we stress that these equations should be prescribed only within the volume enclosed below the Cold-temperate Transition Surface or CTS [Greve (1997)].

We now look to the conservation of energy equation derived in §2.2 and adapt it so that it can be applied to this new setting. Combining (**??**) and (**??**) we have

$$\varphi \rho_f \frac{D_f U_f}{Dt} + (1-\varphi)\rho_m \frac{D_m U_m}{Dt} = \Gamma \Delta U + Q - \nabla \cdot \mathbf{q} - P \nabla \cdot \bar{\mathbf{v}} + \Psi, \tag{3.10}$$

with Ψ defined in (**??**).



(a) Results of 3D X-ray microtomography of magma-mantle flow [Zhu et al. (2011)],

(b) Our proposition: water flowing through viscously deforming polycrystalline ice.

Figure 3.1: Applying coupled magma-mantle dynamics to coupled ice-water flow. A. $\varphi = 0.02$, B. $\varphi = 0.05$, C. $\varphi = 0.10$, D. $\varphi = 0.20$.

There are a few simplifications that we can make at this stage since we're specifically interested in investigating a closed system at equilibrium. Assuming equilibrium dynamics is quite reasonable since we know we're interested in applying these equations to temperate zones, and for a given pressure p, T is therefore fixed at the pressure-melting point. We will also ignore internal heat production as well as heating from the boundary (such as geothermal heating) in these regions: $Q = 0$, and recalling Fourier's law of thermal conduction as $\mathbf{q} = -k\nabla T$, we can see that: $\mathbf{q} = \mathbf{0}$ necessarily, since T is roughly constant, assuming only small changes in p.

Further, since infinitesimal changes in the internal energies dU_i are given by $dU_i = \rho_i c_p^i dT$ where c_p^i is the specific heat capacity of the i^{th} phase, all derivatives involving dU_i must also be negligible at equilibrium. We again stress that this assumption will be useful to us only when considering flow enclosed within the CTS located at the base of ice-stream margins, but will become an increasingly poor supposition as we move further away from these margins and the porosity becomes very small. Above the CTS the single-phase Stokes regime will continue to provide a very good approximation to the flow. Within the region bounded by the CTS the two-phase conservation of energy equation reduces to

$$0 = \Gamma \Delta U - P \nabla \cdot \bar{\mathbf{v}} + \Psi. \tag{3.11}$$

At this stage, since temperature doesn't feature in this conservation equation, one might wonder where all of the energy of this system ends up if it doesn't go into increasing the temperature. The answer lies in the distinction between *sensible heat*, a temperature-changing release of energy which may be "sensed" by a thermometer, and *latent heat*, the energy released in a constant temperature process which is often associated with phase changes [Perrot (1998)]. This explains why all of the viscous dissipation should result in the production of latent heat, leading to melting. In this case we are investigating the process of melting ($\Gamma > 0$), which is

an endothermic reaction. Therefore any energy produced ΔU is then absorbed by the latent heat of fusion of ice. Essentially, although there is no change in the temperature T, i.e. there is no transfer of sensible heat, there is still a transfer of latent heat.

One further simplification comes from applying the Boussinesq approximation (**??**) (here $\nabla \cdot \bar{\mathbf{v}} = 0$ since the right hand side of (**??**) vanishes), then writing $\Delta U = -\mathcal{L}$, (**??**) simply becomes

$$\mathcal{L}\Gamma = \Psi. \tag{3.12}$$

Here $\mathcal{L}$ is the specific latent heat. We can see that given our assumptions, all melting within the temperate region is due solely to dissipation. This new relation for Γ effectively closes the system of thermo-mechanical equations that govern this multi-phase flow.

Hence the full set of equations describing temperate ice-water dynamics with some ice velocity $\mathbf{u}_m$ and water velocity $\mathbf{u}_f$ is given as (**??**)-(**??**). All involved quantities will refer to ice rather than the mantle from now on:

$$\Gamma = \frac{\partial \rho_f \varphi}{\partial t} + \nabla \cdot (\rho_f \varphi \mathbf{u}_f), \tag{3.13}$$

$$-\Gamma = \frac{\partial \rho_m (1-\varphi)}{\partial t} + \nabla \cdot (\rho_m (1-\varphi) \mathbf{u}_m), \tag{3.14}$$

$$\nabla P_f = \nabla \cdot \eta (\nabla \mathbf{u}_m + (\nabla \mathbf{u}_m)^T) + \nabla \left[\left(\zeta - \frac{2\eta}{3} \right) \nabla \cdot \mathbf{u}_m \right] + \rho \mathbf{g}, \tag{3.15}$$

$$\varphi(\mathbf{u}_f - \mathbf{u}_m) = -\frac{K}{\mu} \nabla (P_f + \rho_f g z), \tag{3.16}$$

$$\Gamma = \frac{\mu \varphi^2}{\mathcal{L} K} (\mathbf{u}_f - \mathbf{u}_m)^2 + \frac{\zeta}{\mathcal{L}} (\nabla \cdot \mathbf{u}_m)^2 + \frac{\eta}{2\mathcal{L}} \left(\nabla \mathbf{u}_m + (\nabla \mathbf{u}_m)^T - \frac{2}{3} \mathbb{I} (\nabla \cdot \mathbf{u}_m) \right)^2. \tag{3.17}$$

Equations (**??**)-(**??**) are the result of modifying the cold ice model equations (**??**)-(**??**) by allowing for energy and mass transfer between the two phases; ice and water. Note that (**??**)-(**??**) reduces to these cold ice equations in the limit of zero melting and zero porosity.

3.1 Modelling the Laboratory Experiment

We have now made a few simplifications to the McKenzie equations in order to more accurately apply them to model the dynamics within temperate zones. This framework is, however, still rather abstract and poses a number of difficult questions when applied to the problem at hand. How do we define the boundaries of an ice-stream margin and the CTS? What sort of conditions should we impose on these boundaries? And once we have our results, how could we test them?

To answer these questions and to investigate the mathematical behaviour of these equations whether they are an appropriate description of temperate ice or not, we wish to apply them to a planned experimental setup. Using similar apparatus to that used by Iverson & Peterson

(2011), the design mimics glacial conditions and reproduces ice deformation in order to infer its texture and rheology. The experiment consists of an annular aluminium chamber which holds a ring of temperate ice-water mixture maintained at the pressure-melting temperature in a sealed room. Vertical and horizontal stresses are applied, and water is drained through a permeable interface at the base of the chamber, reproducing the effects of compaction, drainage and shear dissipation. The ring's outermost diameter is 0.9m across and stands at 0.24m in height, as demonstrated in Figure 3.2.

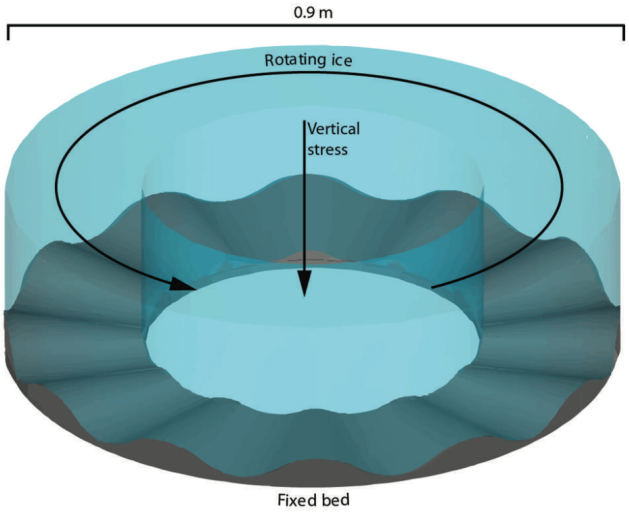


Figure 3.2: We consider a modification of this design, allowing for meltwater drainage through a permeable base [Zoet & Iverson (2015)].

Due to the apparatus' annular symmetry, we may model the ice behaviour effectively in two or even one dimension(s). Taking a Cartesian coordinate system centered on a point at the base of the chamber with the z-axis pointing upwards, parallel to the cylinder axis, the x-axis pointing in the direction of shearing (horizontal stress) and the y-axis pointing towards the center of the chamber, we focus on a 1D column of the ice-water mixture. Taking $\mathbf{u}_i = (u_i, v_i, w_i) \in \mathbb{R}^3$, we set $z = 0$ at the base of the chamber, where the bed is fixed, and $z = H(t)$ at the top of the chamber where the mixture undergoes compression, with $H(t)$ an unknown but monotonically decreasing function of time. Equations (**??**)-(**??**) have now been considerably simplified, and can be expressed as a set of 6 PDEs (as well as the trivial result of Darcy's law in the x-direction: $u_f = u_m$):

$$\frac{\Gamma}{\rho} = \frac{\partial \varphi}{\partial t} + \frac{\partial}{\partial z}(\varphi w_f), \tag{3.18}$$

$$\frac{\Gamma}{\rho} = \frac{\partial \varphi}{\partial t} - \frac{\partial}{\partial z}((1-\varphi) w_m), \tag{3.19}$$

$$\frac{\partial P}{\partial z} = \frac{\partial}{\partial z}\left(\xi \frac{\partial w_m}{\partial z}\right), \tag{3.20}$$

$$\varphi(w_f - w_m) = -\frac{K}{\mu}\frac{\partial P}{\partial z}, \tag{3.21}$$

$$0 = \frac{\partial}{\partial z}\left(\eta \frac{\partial u_m}{\partial z}\right), \tag{3.22}$$

$$\Gamma = \frac{\mu}{\mathcal{L}K}\left[\varphi(w_f - w_m)\right]^2 + \frac{\eta}{\mathcal{L}}\left(\frac{\partial u_m}{\partial z}\right)^2 + \frac{\xi}{\mathcal{L}}\left(\frac{\partial w_m}{\partial z}\right)^2, \tag{3.23}$$

along with the boundary and initial conditions

$$u_m(0,t)=0,\quad w_m(0,t)=0,\quad \varphi(z,0)=\varphi_0,\quad \sigma_{zx}(H,t)=\eta\frac{\partial u_m}{\partial z}(H,t)=\tilde{\sigma}_{zx},$$
$$\sigma_{zz}(H,t)=-P(H,t)+\xi\frac{\partial w_m}{\partial z}(H,t)=\tilde{\sigma}_{zz},\quad \frac{\partial P}{\partial z}(H,t)=0,\quad P(0,t)=0,$$

with $\xi=\zeta+4\eta/3$ as the compaction viscosity. Here we take the ice weight ($\rho gV\sim 10^3$N) to be negligible compared to the vertical compaction stresses induced by the apparatus ($\sigma A\sim 10^5$N). Since the densities of ice and water are of a similar magnitude, with both quantities exhibiting little variation in space and time, we take them to be constant, uniform and equal to one another: $\rho_f=\rho_m=\rho$. Before the vertical shear stress is first applied to the ice-water mixture in the experiment, the porosity can be controlled and is therefore set to be approximately to uniform at $t=0$, yielding the initial condition $\varphi(z,0)=\varphi_0$. Finally, we utilise the equilibrium constitutive law for two-phase flows $P=P_f$ [Rudge et al. (2011)].

Note that we must have 6 PDEs for 6 unknowns: $w_f(z,t)$, $w_m(z,t)$, $u_m(z,t)$, $\Gamma(z,t)$, $\varphi(z,t)$ and $P(z,t)$ with all other quantities either constant, or functions of these unknowns. We will use a no-slip condition $u_m(0,t)=u_f(0,t)=0$ at the base, which itself is permeable to water but not to ice, i.e. $w_m(0,t)=0$. The initial porosity is assumed to be uniform: $\varphi(z,0)=\varphi_0$ and the boundary conditions $\sigma_{zx}(H,t)=\eta\partial_z u_m(H,t)=\tilde{\sigma}_{zx}$ and $\sigma_{zz}(H,t)=-P(H,t)+\xi\partial_z w_m(H,t)=\tilde{\sigma}_{zz}$ for some constant prescribed stresses $\tilde{\sigma}_{zx}$, $\tilde{\sigma}_{zz}$, are derived from (**??**). Finally, we assume a constant pressure (chosen to be zero) at the ice-bed interface $P(0,t)=0$, and since $w_f=w_m$ at the top of the column, (**??**) demands that we have a zero pressure gradient at this point: $\partial_z P(H,t)=0$.

3.2 The Non-dimensionalised Equations

We now have a set of simplified PDEs along with boundary conditions that can be used to model temperate ice-water flows in one dimension. Our next step is to simplify the forms of (**??**)-(**??**) further by *non-dimensionalising* them, that is, by making each independent variable dimensionless. This will also help us to recover characteristic properties of the system. We introduce the following transformations

$$w_i=\left(\frac{\rho\mathcal{L}H_0}{\xi_0}\right)\hat{w}_i,\quad u_i=\left(\frac{\rho\mathcal{L}H_0}{\eta_0}\right)\hat{u}_i,\quad z=H_0\hat{z},\quad t=\left(\frac{\xi_0}{\rho\mathcal{L}}\right)\hat{t},\quad K=K_0\hat{K},$$
$$\xi=\xi_0\hat{\xi},\quad \eta=\eta_0\hat{\eta},\quad P=\left(\frac{\mu\rho\mathcal{L}H_0^2}{\xi_0K_0}\right)\hat{P},\quad \sigma_{ij}=\left(\frac{\mu\rho\mathcal{L}H_0^2}{\xi_0K_0}\right)\hat{\sigma}_{ij},\quad \Gamma=\left(\frac{\rho^2\mathcal{L}}{\xi_0}\right)\hat{\Gamma},$$

and choose $\xi_0=\eta_0$.

$$\Gamma = \frac{\partial \varphi}{\partial t} + \frac{\partial}{\partial z}(\varphi w_f), \tag{3.24}$$

$$\Gamma = \frac{\partial \varphi}{\partial t} - \frac{\partial}{\partial z}((1-\varphi) w_m), \tag{3.25}$$

$$\mathcal{R}^2 \frac{\partial P}{\partial z} = \frac{\partial}{\partial z}\left(\xi \frac{\partial w_m}{\partial z}\right), \tag{3.26}$$

$$\varphi(w_f - w_m) = -K \frac{\partial P}{\partial z}, \tag{3.27}$$

$$0 = \frac{\partial}{\partial z}\left(\eta \frac{\partial u_m}{\partial z}\right), \tag{3.28}$$

$$\Gamma = \mathcal{R}^2 \frac{1}{K}\left[\varphi(w_f - w_m)\right]^2 + \eta\left(\frac{\partial u_m}{\partial z}\right)^2 + \xi\left(\frac{\partial w_m}{\partial z}\right)^2, \tag{3.29}$$

$$u_m(0,t) = 0, \quad w_m(0,t) = 0, \quad \varphi(z,0) = \varphi_0, \quad \sigma_{zx}(H/H_0,t) = \frac{1}{\mathcal{R}^2}\eta \frac{\partial u_m}{\partial z}(H/H_0,t) = \tilde{\sigma}_{zx},$$

$$\sigma_{zz}(H/H_0,t) = -P(H/H_0,t) + \frac{1}{\mathcal{R}^2}\xi \frac{\partial w_m}{\partial z}(H/H_0,t) = \tilde{\sigma}_{zz}, \quad \frac{\partial P}{\partial z}(H/H_0,t) = 0, \quad P(0,t) = 0.$$

Substituting these into equations (**??**)-(**??**) and dropping the hats gives us our reduced equations in non-dimensional form, along with the above boundary and initial conditions.

Here $\mathcal{R} = H_0/\sqrt{\xi_0 K_0/\mu}$ is a dimensionless parameter which represents the ratio between two different length-scales associated with the experiment. $H(0) = H_0$ is the initial height of our ice column and $\sqrt{\xi_0 K_0/\mu}$ is a quantity with dimensions of length which we will call the *compaction length*. We write

$$\delta \equiv \sqrt{\frac{\xi_0 K_0}{\mu}}. \tag{3.30}$$

Compaction is the process by which the ice matrix progressively loses its porosity due to external stresses, and the compaction length is the distance over which compaction effects penetrates into the mixture. Varying δ changes the physics of this experiment significantly, and we will investigate one of the limiting cases in detail later on in this report. In addition, we denote the compaction rate $\mathcal{C}$ and define it as

$$\mathcal{C} \equiv -\nabla \cdot \mathbf{v}_m = -\frac{\partial w_m}{\partial z}. \tag{3.31}$$

3.3 Constitutive Laws & Experimental Values

Some work has been done on the constitutive laws of ice flow, and as discussed, the effects of meltwater on ice deformation have also been investigated [Duval (1977); Piazolo et al. (2013)] with a statement of energy conservation proposed for polythermal ice sheets [Aschwanden et al. (2012)]. Within this field, however, much remains to be validated and confirmed by observation, and given this, we will aim to derive our constitutive relations from experimental data retrieved from mantle rocks. This should help us to make informed decisions regarding our glaciological prescriptions under the assumption that ice possesses a similar rheology. This seems reasonable

to us given our understanding of geological crystal structure and deformation in both the mantle and in ice sheets.

First, consider the permeability. This must of course depend on the porosity of the mixture: the higher the porosity, the greater the pore space within the ice matrix and the easier it becomes for the water to flow. We suppose that the permeability follows a power law relation,

$$K = K_0 \left(\frac{\varphi}{\varphi_0}\right)^{\alpha} = \frac{d^2}{\gamma}\left(\frac{\varphi}{\varphi_0}\right)^{\alpha}, \tag{3.32}$$

where d is the average grain size (usually between 1 and 10mm for ice), presumed constant, $\varphi_0 = \varphi(z,0)$ and γ is a geometric factor which depends on the dihedral angle, also constant. Note that when $\varphi = \varphi_0$, $K = K_0$. For mantle rocks, the exponent $\alpha = 2.6 \pm 0.2$ is based on experiment, [Miller et al. (2013)] and for ice α is similarly derived; commonly taken to be equal to 3 [Cuffey & Paterson (2010)].

For single-phase flows we saw that the effective shear viscosity $\eta = \eta(T,\tau)$ was a function of both the temperature and the stress state. For two-phase flows we more generally have $\eta = \eta(T,\tau,\varphi)$, since the viscosity will now depend on the concentrations of each of the two phases within the mixture. For simplicity, here we will concentrate on stress-independent (i.e. Newtonian) viscosities, and assume a porosity-weakening rheology of the form $\eta(\varphi) = \eta_0 e^{-\lambda(\varphi-\varphi_0)}, \lambda \in \mathbb{R}^+$ since we are currently only interested in temperate ice, where T is fixed at the pressure-melting temperature. The compaction viscosity scales similarly to the effective shear viscosity modulo a multiplicative factor proportional to φ^{-m}: $\xi(\varphi) = \xi_0 e^{-\lambda(\varphi-\varphi_0)}(\varphi/\varphi_0)^{-m}$, $m \in \mathbb{R}^+$, where m is usually taken to be equal to 1, as in Simpson et al. (2010).

Quantity	Symbol	Experimental Value	Units
Compaction viscosity const.	ξ_0	2×10^{15}	Pa s
Shear ice viscosity const.	η_0	2×10^{13}	Pa s
Water viscosity	μ	8.90×10^{-4}	Pa s
Geometric factor	γ	58	
Permeability exponent	α	3	
Compaction exponent	m	1	
Specific latent heat of fusion	$\mathcal{L}$	3.35×10^5	J m^{-3} kg^{-1}
Density of glacier ice	ρ_m	9.17×10^2	kg m^{-3}
Density of water	ρ_f	1×10^3	kg m^{-3}
Viscosity const.	λ	27	

Table 3.1: Dimensional parameters used in the model and their experimentally-derived values.

In running the model, we will be looking to evaluate the qualitative behaviour of the system, but we will also be interested in quantifying the system's responses so that these can be tested and verified by experimentalists. To this end, we use the following parameter values in Table 3.1, taken from Weast (1981), Fowler (2013) and Katz (2015), where the value of the compaction viscosity constant assumes an average porosity of 0.01. These experimental values will be used from now on, unless explicitly stated otherwise.

Chapter 4

Instantaneous Compaction

4.1 Instantaneous Equations

Since the initial porosity is set to be uniform, we can formulate an "instantaneous" or time-independent compaction problem at time $t = 0$, neglecting all time derivatives, with $\varphi = \varphi(z, 0)$. This further simplifies and decouples the model set of PDEs derived in §3.2 so that the behaviour of the system can now be captured by the 4 non-dimensionalised mechanical ODEs: (**??**)-(**??**). Non-dimensionally we now have $\eta = 1$, $K = 1$, $\xi = 1$, all assumed uniform i.e. independent of z. This reduced set of equations becomes

$$\mathcal{R}^2 \frac{dP}{dz} = \frac{d^2 w_m}{dz^2}, \tag{4.1}$$

$$\frac{dw_m}{dz} = \frac{d^2 P}{dz^2}, \tag{4.2}$$

$$\frac{dP}{dz} = -\varphi_0 (w_f - w_m), \tag{4.3}$$

$$0 = \frac{d^2 u_m}{dz^2}, \tag{4.4}$$

with boundary conditions

$$u_m(0,0) = 0, \quad w_m(0,0) = 0, \quad \sigma_{zz}(1,0) = -P(1,0) + \frac{1}{\mathcal{R}^2}\frac{dw_m}{dz}(1,0) = \tilde{\sigma}_{zz},$$

$$\sigma_{zx}(1,0) = \frac{1}{\mathcal{R}^2}\frac{du_m}{dz}(1,0) = \tilde{\sigma}_{zx}, \quad \frac{dP}{dz}(1,0) = 0, \quad P(0,0) = 0.$$

Let's start with equation (**??**), which is straightforward to solve in this case: $u_m(z) = u_f(z) = \mathcal{U}z$, where $\mathcal{U} = \mathcal{R}^2 \tilde{\sigma}_{zx}$ is a dimensionless shearing velocity. Therefore taking a snapshot of the experiment at $t = 0$ reveals a Couette flow in the x-direction, exemplifying simple shear. Considering equations (**??**) and (**??**), we remark that we are now in possession of a coupled system of two ODEs for $w_m(z)$ and $P(z)$, and along with the relevant boundary conditions we have an example of what is known as a "Filter Press" problem.

4.2 The Filter Press Problem

A Filter Press problem models a 1D column of fluid mixture, whereby some normal stress is applied to an impermeable lid at the top of the column. This pushes the contents downwards, compacting the mixture and forcing one or more of the constituent fluids through a permeable interface at the base. This is similar to how a French Press filters hot water while remaining impermeable to the ground coffee beans. In this problem, however, water is drained through the surface at the base of the column and the ice becomes further compacted within. A schematic diagram of this setup is shown in Figure 4.1.

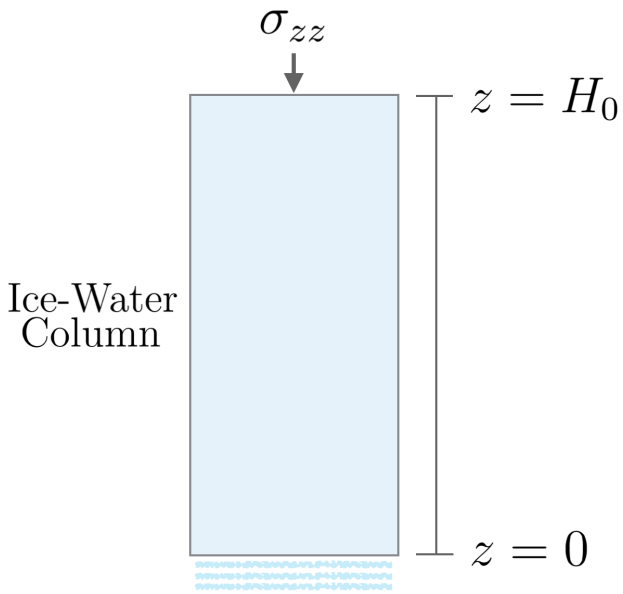


Figure 4.1: The Filter Press Problem setup.

We will assume a vertical stress σ_{zz} to act on the mixture, as per the boundary conditions set out in §4.1, though in the instantaneous case considered here we will fix a vertical velocity component $\mathcal{W}$ and then calculate the stress corresponding to that velocity. That is, we will imagine compressing the impermeable lid downwards at a constant velocity $-\mathcal{W}$. With this condition in place, equations (**??**) and (**??**) may be solved analytically to yield the instantaneous non-dimensional pressure distribution (**??**) and instantaneous non-dimensional ice velocity profile (**??**). We then use (**??**) to obtain the instantaneous water velocity profile (**??**).

$$P(z) = \frac{\mathcal{W}}{\mathcal{R}}\left[\frac{\cosh\mathcal{R} - \cosh\mathcal{R}(1-z)}{\sinh\mathcal{R}}\right], \tag{4.5}$$

$$w_m(z) = \mathcal{W}\left[\frac{\sinh\mathcal{R}(1-z)}{\sinh\mathcal{R}} - 1\right], \tag{4.6}$$

$$w_f(z) = \mathcal{W}\left[\left(1 - \frac{1}{\varphi_0}\right)\frac{\sinh\mathcal{R}(1-z)}{\sinh\mathcal{R}} - 1\right], \tag{4.7}$$

$$u_m(z) = u_f(z) = \mathcal{U}z. \tag{4.8}$$

Note that here $\mathcal{W}$ has been introduced into the solutions as a dimensionless velocity. The above results may be combined into a vector plot of $\{\mathbf{u}_i\}$, which is shown in Figure 4.2. Expanding into the x-direction, this demonstrates an approximate snapshot of the ice/water velocity profiles within a 2D element inside the apparatus chamber at $t = 0$, according to the model.

In Figure 4.2 $\mathcal{U}$, $\mathcal{W}$ and $\mathcal{R}$ are all set equal to 1, the latter indicating that the compaction length δ has been set equal to the initial chamber height H_0, a condition that corresponds physically to the compaction effects penetrating through the entire column. This vertical advection profile reflects and is supported by much of the literature [Cuffey & Paterson (1969), Zotikov

(1986), Jacobson & Raymond (1998)]. Glacial compaction effects are observed over a large range of length-scales however, and so we may wish to experiment with different possible values for $\mathcal{R}$. Figure 4.3 shows how such experimentation with $\mathcal{R}$ (set equal to 0.1, 1 and 10) produces a range of qualitatively different results. To be clear, $\mathcal{R} = 10$ corresponds to $\delta = H_0/10$, that is, compaction only penetrates 1/10 of the way downwards through the column from the surface. Taking the limit $\mathcal{R} \to 0$, which is equivalent to considering an "infinite compaction length" δ with H_0 held fixed, simplifies things even further. For example, we can take the small $\mathcal{R}$ limit of (??) to give

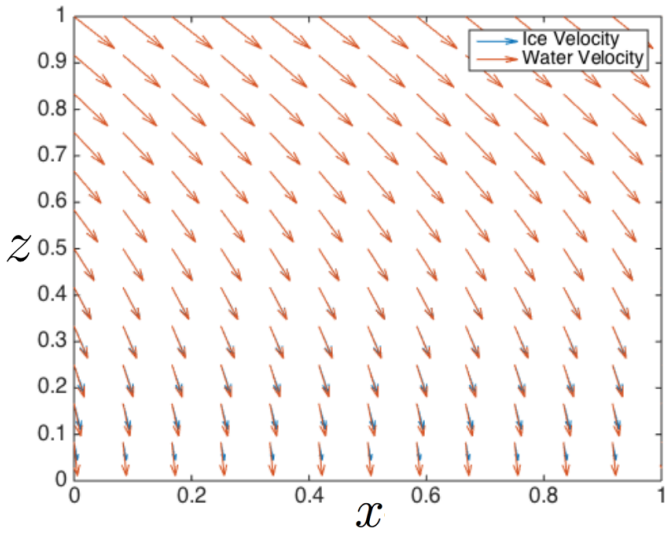


Figure 4.2: Ice & water 2D velocity profiles. $\mathcal{U} = \mathcal{W} = 1$.

$$\lim_{\mathcal{R}\to 0} \mathcal{W}\left[\frac{\sinh \mathcal{R}(1-z)}{\sinh \mathcal{R}} - 1\right] = -\mathcal{W}z.$$

This result is in agreement with both the literature and the plots in Figure 4.3b), since we can see that as $\mathcal{R}$ gets progressively smaller, the gradient of the curve becomes closer and closer to -1 (with $\mathcal{W} = 1$). Recalling the mathematical definition of the compaction rate (??) and non-dimensionalising, we find that in this limit $\mathcal{C} = \mathcal{W} = const.$ i.e. the ice-water mixture feels the effects of compaction equally for all z at $t = 0$ since δ is infinite. And this is exactly what we observe in Figure 4.3b). In the limit $\mathcal{R} \to 0$, a constant compaction rate implies that the porosity will evolve independently of z. That is, it will remain uniform for all time. In this case, the analysis in this chapter holds not only for small times, but for all times, provided that the initial porosity is uniform.

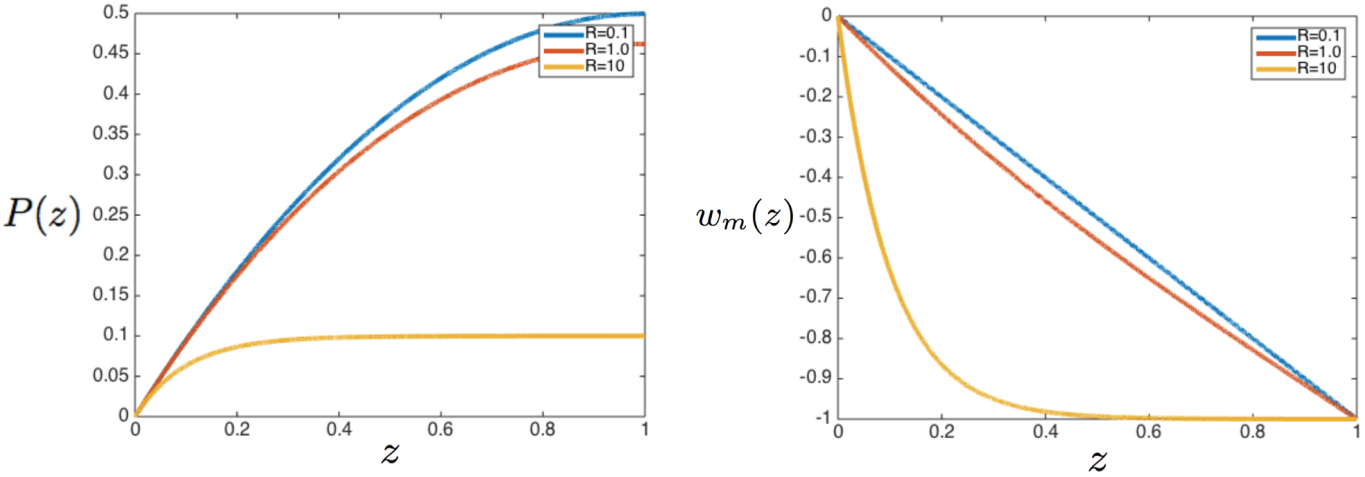
A constant velocity $-\mathcal{W}$ was prescribed in this section in place of a constant stress $\tilde{\sigma}_{zz}$ in the small $\mathcal{R}$ limit. More generally however, for any $\mathcal{R}$, the corresponding normal stress needed in order to force the top of the column downwards at a speed $\mathcal{W}$ can be found from the form of the dimensionless bulk stress tensor (??) at $t = 0$:

$$\sigma_{zz} = -P(z) + \frac{1}{\mathcal{R}^2}\frac{dw_m}{dz}(z), \tag{4.9}$$

$$= -\frac{\mathcal{W}}{\mathcal{R}}\coth \mathcal{R}, \tag{4.10}$$

dropping the hats. Note that the stress is defined as positive upwards, and hence here it is a negative quantity, and independent of z. We will use this definition of the stress tensor when further investigating the infinite compaction length approximation in the next chapter.

It is worth noting that with these instantaneous equations, the melt rate does not affect the dynamics, though it is still useful to derive the small $\mathcal{R}$ limit of equation (??), given by



(a) Non-dimensionalised $P(z)$ vs. z,

(b) Non-dimensionalised $w_m(z)$ vs. z.

Figure 4.3: The non-dimensionalised solutions (??) and (??), plotted for $\mathcal{R} = 0.1, 1, 10$.

$$\Gamma = \mathcal{R}^2 K \left(\mathcal{W} \frac{\sinh \mathcal{R}(1-z)}{\sinh \mathcal{R}} \right)^2 + \eta \mathcal{U}^2 + \xi \left(-\mathcal{W}\mathcal{R} \frac{\cosh \mathcal{R}(1-z)}{\sinh \mathcal{R}} \right)^2, \tag{4.11}$$

so that it can be used in the next chapter. Then, formally taking the limit $\mathcal{R} \to 0$, the first term on the right hand side vanishes and the third term reduces to a constant, giving

$$\Gamma = \eta \mathcal{U}^2 + \xi \mathcal{W}^2. \tag{4.12}$$

Chapter 5

Infinite Compaction Length Approximation

In §4.2 we introduced the idea of an "infinite compaction length" approximation, that is, an approximation to the equations where the ratio $\mathcal{R} = H_0/\delta$ is taken to be very small. In Chapter 5, we are going to focus on this limiting case, finding both analytical and numerical solutions to the model's time-dependent set of equations. We will also be interested in quantifying the behaviour of these solutions and so in this chapter we revert to using dimensional forms.

5.1 Evolution of Porosity by Compaction

Intending to keep the physics relatively simple at this stage, we will neglect all melting in the column ($\Gamma = 0$), focussing on the Filter Press Problem we encountered in §4.2. Equation (**??**) then gives us a dimensional statement of mass conservation for ice, which may be expanded as

$$\frac{\partial \varphi}{\partial t} + w_m \frac{\partial \varphi}{\partial z} = (1-\varphi)\frac{\partial w_m}{\partial z}. \tag{5.1}$$

We saw in Chapter 4 that the compaction rate $\mathcal{C} = -w_m'(z)$ became independent of z in the limit of small $\mathcal{R}$. Given an initial uniform porosity, this implies that the porosity will evolve independently of z for all times t i.e. $\varphi = \varphi(t)$ only. Specifically, $w_m'(z) = -\mathcal{W}/H_0$ and therefore

$$\frac{d\varphi}{dt} = -\frac{\mathcal{W}}{H}(1-\varphi), \tag{5.2}$$

an ODE for $\varphi(t)$. Note that we have replaced H_0 with $H = H(t)$ to allow the column height to vary as a function of time. The most simple non-trivial prescription for $H(t)$ fixes $\mathcal{W}$, implying $H(t) = H_0 - \mathcal{W}t$, providing a solution to (**??**):

$$\varphi(t) = 1 - \frac{H_0(1-\varphi_0)}{H_0 - \mathcal{W}t}. \tag{5.3}$$

This can be thought of as an equivalent statement of mass conservation: $H(1-\varphi) = H_0(1-\varphi_0)$.

The Filter Press Problem models the effects of compaction, and so, like $H(t)$, we expect the porosity $\varphi(t)$ to be a monotonically decreasing function of t, which according to (**??**) it

is. Imposing a constant vertical velocity isn't a particularly easy constraint for us to replicate experimentally, however. As the ice-water mixture is compressed, its constituent molecules are pushed closer and closer together, bonding more tightly and cumulatively exerting a greater pressure on their surroundings. As the mixture continues to compact, the effective viscosity will increase indefinitely and a constant vertical velocity would eventually require an infinite amount of energy to maintain such a compression. Mathematically speaking, we can also see that (**??**) will eventually break down as with $H_0, 1-\varphi_0$ being positive, this means that $t > H_0/\mathcal{W}$ implies $\varphi > 1$, a contradiction. Physically, the chamber would contract to a volume $V = 0$ at $t = H_0/\mathcal{W}$ and the model would then become invalid for all greater t.

In fact, imposing a constant stress is a simple constraint for us to implement in our experiment, via a constant load, for example. The non-dimensional normal stress required to maintain a constant compaction velocity is given by (**??**). Here however, we wish to relate the constant vertical stress $\tilde{\sigma}_{zz}$ to the velocity $\mathcal{W}(t) = -dH/dt$. In order to recover the term $\mathcal{W}$ we re-dimensionalise $\tilde{\sigma}_{zz}$ in the limit $\mathcal{R} \to 0$, writing

$$\frac{dH}{dt} = \frac{\tilde{\sigma}_{zz} H}{\xi_0}. \tag{5.4}$$

Separation of variables then gives us the solution

$$H = H_0 e^{\frac{-|\tilde{\sigma}_{zz}|}{\xi_0} t}, \tag{5.5}$$

an exponential decay, plotted in Figure 5.1a). An exponential decay in height under constant stress much more closely mimics the kind of physical behaviour we might expect of ice deformation, but we still have a similar problem to the simplified case outlined above. Here we are neglecting melt rate, yet (**??**) requires $H(t) \to 0$ as $t \to \infty$, seeming to require that all of the ice should melt into water, which is then expelled through the permeable chamber base.

An exponential decay, therefore, cannot be physical since the only other option for the ice is to undergo an infinite amount of compression. Mass conservation tells us that $\lim_{t\to\infty} H(t) = H_0(1-\varphi_0)$, a quantity which may only ever reach 0 in the case where $\varphi(0) = \varphi_0 = 1$, i.e. when the ice-water mixture is in fact entirely water.

In Chapter 4, we commenced by assuming $K = K_0$, $\eta = \eta_0$ and $\xi = \xi_0$ (dimensionally) to be constant, but from now on we will take these quantities to follow the constitutive laws laid out in Chapter 3: $K = K_0(\varphi/\varphi_0)^\alpha$, $\alpha \geq 1$, $\eta = \eta_0 e^{-\lambda(\varphi-\varphi_0)}$, $\lambda \in \mathbb{R}^+$ and $\xi = \xi_0 e^{-\lambda(\varphi-\varphi_0)}(\varphi/\varphi_0)^{-m}$, $m \in \mathbb{R}^+$. Note that we are still neglecting the grain size evolution $\dot{d}$, which is specified by the constant K_0.

Replacing ξ_0 with ξ in (**??**) and imposing mass conservation (equation (**??**)) gives

$$\frac{\tilde{\sigma}_{zz}}{\varphi_0^m \xi_0}\varphi^m = \frac{1}{1-\varphi}\frac{d\varphi}{dt}, \tag{5.6}$$

where we have assumed that $\lambda(\varphi - \varphi_0) \ll 1$. Separation of variables yields the following integral equation:

$$\frac{\tilde{\sigma}_{zz}}{\varphi_0^m \xi_0}\int dt = \int \frac{\varphi^{-m}}{1-\varphi} d\varphi. \tag{5.7}$$

An integral such as the one on the right hand side of (**??**) is usually evaluated in terms of the so-called *hypergeometric function*. Most generally, for some φ with exponent χ

$$\int \frac{\varphi^{-\chi}}{(1-\varphi)}\, d\varphi = -\frac{\varphi^{1-\chi}}{\chi-1}\, {}_2\mathcal{F}_1(\chi, 1-\chi; 2-\chi; \varphi), \tag{5.8}$$

where the hypergeometric function ${}_2\mathcal{F}_1$ is defined by the power series

$${}_2\mathcal{F}_1(q, b; c; \varphi) = \sum_{\alpha=0}^{\infty} \frac{(q)_\alpha (b)_\alpha}{(c)_\alpha} \frac{\varphi^\alpha}{\alpha!}, \tag{5.9}$$

for $|\varphi| < 1$ [Ince (1956)], within our range, and $(\,)_\alpha$ is the rising Pochhammer symbol. The hypergeometric function provides an exact result, although we can in fact retrieve a qualitatively similar yet considerably simpler solution by considering a sufficiently small porosity, typical of glaciological observations. We can then make the approximation $1 - \varphi \approx 1$. In that case equation (**??**) reduces, and assuming $m \neq 1$, it yields the solution

$$\frac{\tilde{\sigma}_{zz}}{\varphi_0^m \xi_0} t = \frac{\varphi^{1-m} - \varphi_0^{1-m}}{1-m}. \tag{5.10}$$

Equally, if $m = 1$, then (**??**) yields the solution

$$\varphi = \varphi_0 e^{-\frac{|\tilde{\sigma}_{zz}|}{\varphi_0^m \xi_0} t}, \tag{5.11}$$

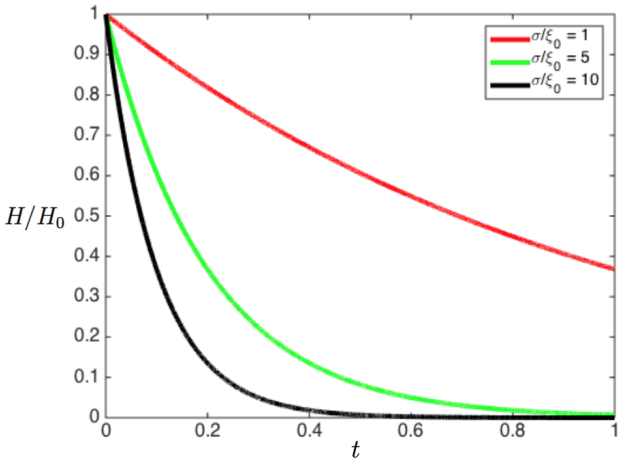
exponential decay, as in (**??**). For $m \neq 1$, we can recast (**??**) in terms of H using $H(1-\varphi) = H_0(1-\varphi_0)$ giving

$$\frac{\tilde{\sigma}_{zz}}{\varphi_0^m \xi_0} t = \frac{\left(1 - \frac{H_0}{H}(1-\varphi_0)\right)^{1-m} - \varphi_0^{1-m}}{1-m}. \tag{5.12}$$

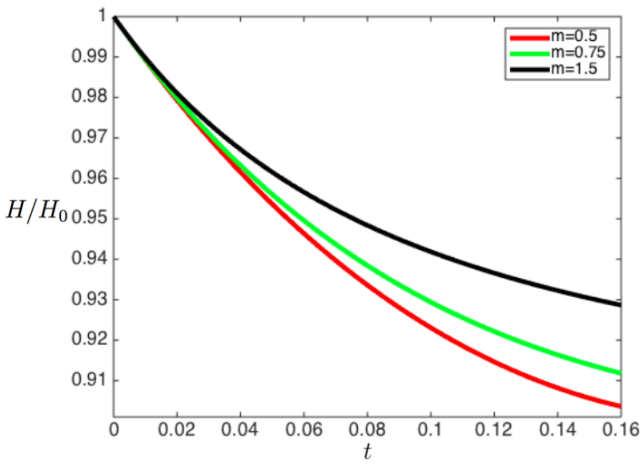
Figure 5.1b) shows H/H_0 plots for a range of values for m, with $\varphi_0 = 0.1$. Note that H/H_0 now asymptotes to $1 - \varphi_0 = 0.9$. This indicates that we could set up our experiment chamber to fully hold a mixture of 10% water and 90% ice, say. When neglecting melting, gravitational forces and density gradients, applying a constant stress to the roof of the chamber would force the water through the viscously deforming ice matrix and out of the permeable base. This process would become slower and slower under a constant stress and would never reduce the height of the chamber by more than 10%, a physically intuitive result.

5.2 Evolution of Porosity by Shearing

In §5.1, we examined the conservation of mass equations, and looked at how they model compaction and drainage in the ice column. We derived an analytical solution for the porosity $\varphi(t)$ and examined how the amount of meltwater present should change in time. However, we also wish to model heating from shear dissipation within the column since as the experimental chamber rotates shear stresses are induced at the boundary and throughout the temperate ice. We briefly looked at simple shear in §4.1 when demonstrating that (**??**) describes a simple Couette flow in the x-direction, assuming a uniform shear viscosity. Here we focus on how $\varphi(t)$



(a) $H(t)/H_0$ from (??),



(b) $H(t)/H_0$ from (??) ($\sigma/\xi_0 = 1$).

Figure 5.1: Comparing $H(t)/H_0$ profiles.

evolves with zero compaction ($\mathcal{C} = 0$) but allowing for shear dissipation. In such a case the model reduces to the following set of PDEs:

$$\Gamma = \rho \frac{\partial \varphi}{\partial t}, \tag{5.13}$$

$$0 = \frac{\partial}{\partial z}\left(\eta \frac{\partial u_m}{\partial z}\right), \tag{5.14}$$

$$0 = \frac{\partial P}{\partial z}, \tag{5.15}$$

$$\Gamma = \frac{\eta}{\mathcal{L}}\left(\frac{\partial u_m}{\partial z}\right)^2, \tag{5.16}$$

with boundary conditions $u_m(0) = 0, u_m(H) = \mathcal{U}$, initial condition $\varphi(0) = \varphi_0$, and prescription for the dimensionless shear viscosity $\eta = \eta_0 e^{-\lambda(\varphi - \varphi_0)}$. Combining equations (??) and (??) then gives us

$$\frac{\partial \varphi}{\partial t} = \frac{\eta_0}{\rho \mathcal{L}} e^{-\lambda(\varphi - \varphi_0)} \left(\frac{\partial u_m}{\partial z}\right)^2, \tag{5.17}$$

and thus, substituting the solution of (??) into (??) yields

$$\varphi = \varphi_0 + \frac{1}{\lambda} \ln(1 + \beta \lambda t). \tag{5.18}$$

Here $\beta = \eta_0 \mathcal{U}^2 / \mathcal{L} H_0^2 \rho$ and we've used that $H \approx H_0$. With the pressure gradient equal to zero, we again see that this simple shear of a two-phase mixture gives rise to a Couette flow where the dissipation drives a logarithmically increasing porosity in time. Note that this is a qualitatively different result to the case in §5.1, where a "compaction only" experiment led to a decreasing porosity in time.

Whether the porosity is decreasing or increasing, we know that both of these toy models are incomplete. In §4.2, although a non-zero melt rate ($\Gamma = 0$) is not specifically prescribed, the model doesn't incorporate porosity evolution by melting. And in §5.1, melting is neglected in the combined conservation of mass equation. Conversely, in §5.2 we have ignored the effects of

compaction and drainage, and so as the ice melts, we observe a continual increase in meltwater. We now want to unify these two reduced models into a combined model in order to remedy these failures, and seek a way to balance the effects of melting and compaction to achieve a steady state porosity.

5.3 The Combined Model

Including compaction, drainage and shear dissipation in one model in order to better describe porosity evolution in the experimental setup can be achieved by combining the dimensional equations (??) and (??). By re-dimensionalising equation (??), we can see that in the small $\mathcal{R}$ limit, this combination reduces to an ODE for $\varphi(t)$:

$$\frac{d\varphi}{dt} + (1-\varphi)\frac{\mathcal{W}}{H} = \frac{\xi \mathcal{W}^2}{\mathcal{L}H^2\rho} + \frac{\eta \mathcal{U}^2}{\mathcal{L}H^2\rho}. \tag{5.19}$$

This equation states that the time evolution of φ depends on the prescribed shear velocity $\mathcal{U}$, compaction velocity $-\mathcal{W}$, and the shear and compaction viscosities η and ξ. The second term on the left hand side is a compaction term. The first term on the right hand side represents *compaction dissipation* in the mixture and the second term represents *shear dissipation*. The relative sizes of these terms will become important when considering which process should dominate and how these processes may be able to balance one another.

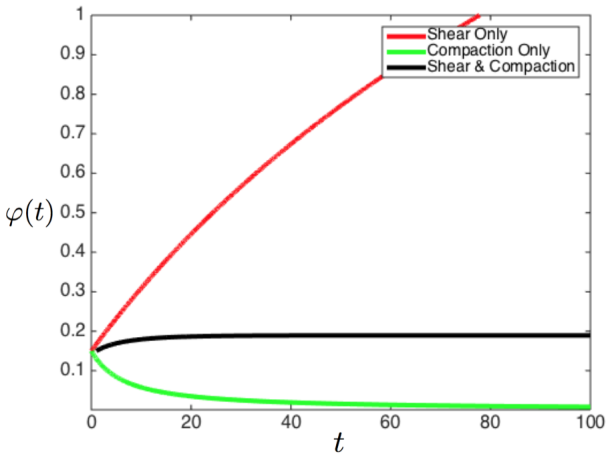


Figure 5.2: $\varphi(t)$ for shear only, compaction only and both.

Finding a stable steady-state solution of (??) would mean that the temperate ice in the experiment could be simultaneously sheared, compacted and drained of meltwater at just the right rates in order to maintain a constant liquid volume fraction within the chamber. Such stability in the amount of meltwater present in these temperate regions, or lack of it, could be of fundamental importance in understanding the reasons for the turning on and off of ice streams and in facilitating margin migration.

Equation (??) can be rewritten using the given prescriptions for η and ξ, allowing us to express each term as a function of φ:

$$\dot{\varphi} = \mathcal{B}_1 \frac{e^{-\lambda\varphi}}{\varphi} + \mathcal{B}_2 e^{-\lambda\varphi} - \mathcal{B}_3(1-\varphi), \tag{5.20}$$

with $\mathcal{B}_1 = \xi_0 \mathcal{W}^2 \varphi_0 e^{\lambda\varphi_0}/\mathcal{L}H_0^2\rho$, $\mathcal{B}_2 = \eta_0 \mathcal{U}^2 e^{\lambda\varphi_0}/\mathcal{L}H_0^2\rho = \beta e^{\lambda\varphi_0}$ and $\mathcal{B}_3 = \mathcal{W}/H_0$, $H \approx H_0$. The solution to (??) can be computed numerically, and the result is plotted in black in Figure 5.2 with $\varphi_0 = 0.15$, $\lambda = 10$, $\mathcal{B}_1 = \mathcal{B}_3 = 100\ \mathrm{s}^{-1}$, $\mathcal{B}_2 = 10\ \mathrm{s}^{-1}$. Note how this result compares

with the compaction-driven porosity solution and the shear dissipation-driven solution: it appears to have provided us with a compromise between the two.

These particular values for the constants in (**??**) were chosen because they produce steady-state trajectories. That is, this particular choice of $\{\mathcal{B}_i, \lambda\}$ produces a solution $\varphi(t)$ that converges on some fixed value φ_e, a solution to (**??**) when $\dot{\varphi} = 0$. The difference in magnitude of the outflux of water through compaction and drainage, and the influx of water through melting vanish as t becomes very large, that is $\dot{\varphi} \to 0$ as $t \to \infty$. Mathematically, we're able find the exact range of possible values $\{\mathcal{B}_i, \lambda\}$ that provide (**??**) with steady-state solutions. The key question is then: do the experimental values found for the constants ξ_0, $\mathcal{L}$, H_0, ρ, η_0 and the other values listed in Table 3.1 produce such $\{\mathcal{B}_i, \lambda\}$? This can be analysed by using some experimentation and stability analysis.

5.4 Stability Analysis

Equation (**??**) belongs to a class of simple ODEs that may be written in the form:

$$\dot{\varphi} = f(\varphi(t)). \tag{5.21}$$

As such, we can introduce a perturbation $\delta\varphi$ around some equilibrium point (or steady-state solution) φ_e, given by $f(\varphi_e) = 0$, which is not necessarily unique, in order to understand the long term behaviour of φ. Substituting $\varphi = \varphi_e + \delta\varphi$ into (**??**) and performing a Taylor expansion about $\varphi = \varphi_e$ gives us

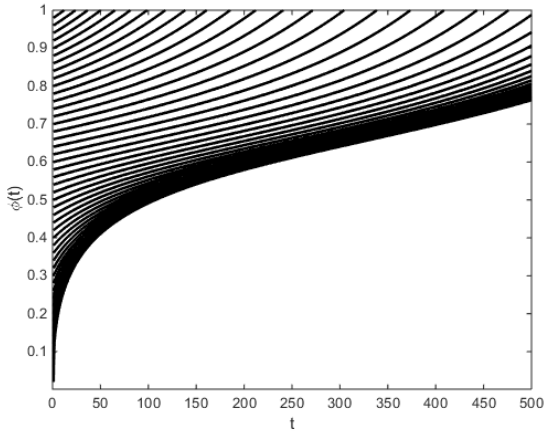
$$\frac{d\varphi_e}{dt} + \frac{d(\delta\varphi)}{dt} = f(\varphi_e + \delta\varphi) = f(\varphi_e) + f'(\varphi_e)\delta\varphi + \mathcal{O}(\delta\varphi^2) \text{ as } \delta\varphi \to 0.$$

Then, neglecting terms of order $\delta\varphi^2$ and above this reduces to

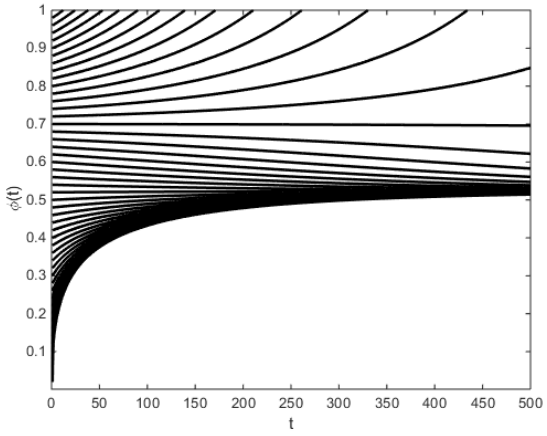
$$\frac{d(\delta\varphi)}{dt} = f'(\varphi_e)\delta\varphi. \tag{5.22}$$

Equation (**??**) can now be used to determine the *linear stability* of a given solution φ_e. We can see that for some small perturbation $\delta\varphi$, the sign of $f'(\varphi_e)$ can tell us whether the solution is either stable or unstable, assuming $f'(\varphi_e) \neq 0$. $f'(\varphi_e) > 0$ corresponds to an unstable solution since a small change in φ leads to an exponential growth away from the steady-state solution φ_e. Conversely, $f'(\varphi_e) < 0$ corresponds to a stable solution since a change in φ leads to an exponential decay towards φ_e.

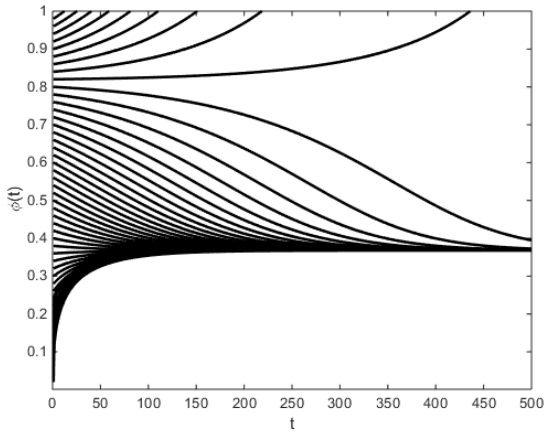
Figure 5.3 demonstrates the emergence of one stable and one unstable steady-state solution to the equation $f(\varphi_e) = 0$. Each figure shows how varying the parameter $\mathcal{B}_3$ affects the existence of steady-state solutions, when starting from a range of different initial porosities $\{\varphi_0\}$. At around $\mathcal{B}_3 = 120$ s^{-1} we see the emergence of a local bifurcation point where we have a transition from no steady-state solutions to two steady-state solutions: one stable and one unstable. At around $\mathcal{B}_3 = 150$ s^{-1}, we start to see more clearly defined steady states with



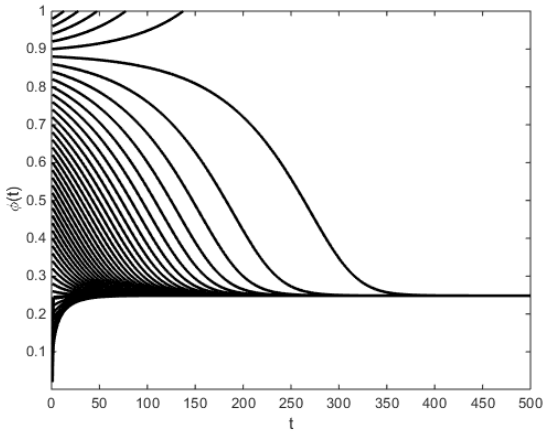
(a) $\mathcal{B}_1 = 50\ \mathrm{s}^{-1}$, $\mathcal{B}_2 = 1\ \mathrm{s}^{-1}$, $\mathcal{B}_3 = 100\ \mathrm{s}^{-1}$.
No steady state solutions exist.



(b) $\mathcal{B}_1 = 50\ \mathrm{s}^{-1}$, $\mathcal{B}_2 = 1\ \mathrm{s}^{-1}$, $\mathcal{B}_3 = 120\ \mathrm{s}^{-1}$.
Steady state solutions emerge from bifurcation point.



(c) $\mathcal{B}_1 = 50\ \mathrm{s}^{-1}$, $\mathcal{B}_2 = 1\ \mathrm{s}^{-1}$, $\mathcal{B}_3 = 150\ \mathrm{s}^{-1}$. $\{\varphi\}$ converge to stable solution $\varphi_e = 0.37$, unstable solution $\varphi_e = 0.81$.



(d) $\mathcal{B}_1 = 50\ \mathrm{s}^{-1}$, $\mathcal{B}_2 = 1\ \mathrm{s}^{-1}$, $\mathcal{B}_3 = 200\ \mathrm{s}^{-1}$. Stable and unstable solutions move further apart as $\mathcal{B}_3$ increases.

Figure 5.3: Emergence of bifurcation point and solutions upon varying the parameter $\mathcal{B}_3$. Each black line is a solution to equation (**??**), starting from a range of different initial porosities between $\varphi_0 = 0.02$ and $\varphi_0 = 0.98$.

stable solution $\varphi_e \approx 0.37$ and unstable solution $\varphi_e \approx 0.81$, in this case.

Furthermore, each term of (**??**) can be made dimensionless simply by dividing the equation through by $\mathcal{B}_3$ and re-scaling time using $\hat{t} = \mathcal{B}_3 t$, yielding an equation of the form

$$\dot{\varphi} = \mathcal{C}_1 \frac{e^{-\lambda\varphi}}{\varphi} + \mathcal{C}_2 e^{-\lambda\varphi} - (1-\varphi), \tag{5.23}$$

where $\mathcal{C}_1 = \mathcal{B}_1/\mathcal{B}_3$, $\mathcal{C}_2 = \mathcal{B}_2/\mathcal{B}_3$ and we've dropped the hat. Taking $f(\varphi)$ to be the right hand side of (**??**), $f(\varphi_e) = 0$ gives us the following equation for stability:

$$1 - \varphi_e = (\frac{\mathcal{C}_1}{\varphi_e} + \mathcal{C}_2) e^{-\lambda\varphi_e}. \tag{5.24}$$

We can now use equation (**??**) to obtain the steady state solutions of (**??**). By substituting in the experimental values detailed in Chapter 3 we're able to identify these solutions graphically, and this is shown by the green-red intersection in Figure 5.4. This intersection gives us $\mathcal{C}_1 = \xi_0 \mathcal{W} \varphi_0 e^{\lambda\varphi_0} / \mathcal{L} H_0 \rho = 27$ and $\mathcal{C}_2 = \eta_0 \mathcal{U}^2 e^{\lambda\varphi_0} / \mathcal{L}\mathcal{W} H_0 \rho = 27$ where $\mathcal{W} = 10^{-9}$ ms^{-1}, $\mathcal{U} = 10^{-8}$ ms^{-1}. At this point it should be noted that this choice of parameters is made for the purposes

of illustration. Although the values of $\mathcal{C}_1$ and $\mathcal{C}_2$ happen to be the same using this choice, this needn't be the case. This yields a stable solution of $\varphi_e = 0.20$, as seen from the graph. To have temperate ice consist of 20% water in the experiment would not be especially reflective as this is a much larger liquid volume fraction than what would typically be observed in the temperate zones of glaciers, and so we conclude that at least one of the following is likely to be true. Either the model is insufficient to accurately describe ice deformation, one of the assumed parameter values is incorrect, or the strain rates are too high for a reasonable steady state to be generated. We will keep these in mind as we continue to investigate the model.

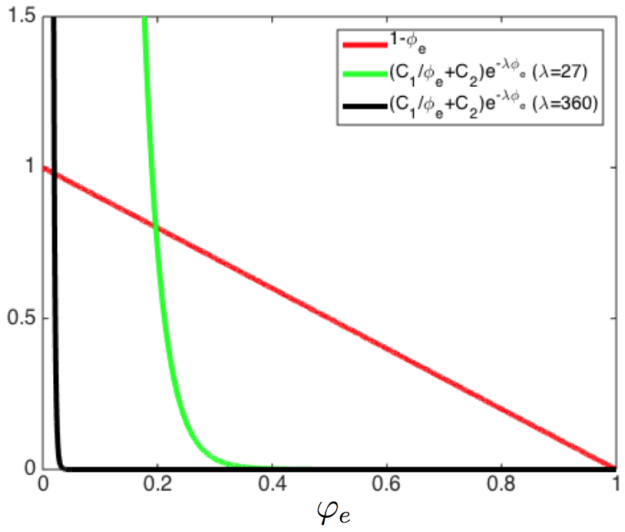


Figure 5.4: Intersections marking steady-state solutions φ_e.

From inspection, the stable solution to (**??**) will decrease monotonically towards zero as the viscosity constant λ tends to ∞. This suggests that if this viscosity constant for ice λ_{ice} were to be much greater than the viscosity constant for mantle rocks λ_{mantle}, a much lower stable steady-state porosity will be observed in the experiment. A stable steady-state porosity of 2%, for example, is achieved by increasing λ to 360, with all other things being equal, and this is shown in Figure 5.4 (black-red intersection). Equally, we could decrease strain rates by decreasing $\mathcal{U}$ and $\mathcal{W}$. With $\lambda = 130$, a decrease in each velocity by a factor of 100 leads to a stable steady state porosity of approximately 2% also. It should be noted, however, that decreasing the strain rates by too much would risk making the experiment unviable. A compaction velocity of $\mathcal{W} = 10^{-11}$ ms^{-1}, for example, would take about 3 years to compact the ice by a millimetre!

If we assume a further simplification at this point, taking the rates of compaction and shear dissipation to be of similar magnitude, ($\mathcal{C}_1 \approx \mathcal{C}_2$), we may graphically represent the above variations by reducing the number of independent variables from 3 to 2. We may now plot $\varphi_e = \varphi_e(\mathcal{C}_1, \lambda)$, a 2D surface made up of all possible steady state solutions, and this is shown in Figure 5.5. The contours of this 2D surface comprise the level set Θ_c of the function φ_e. That is, the contours are given by $\Theta_c(\varphi_e)$ such that $\Theta_c(\varphi_e) = \{(\mathcal{C}_1, \lambda) | \varphi_e(\mathcal{C}_1, \lambda) = c\}$, $c \in \mathbb{R}$ where $f(\varphi_e(\mathcal{C}_1, \lambda)) = 0$. In particular, note that in order to maintain a very small porosity of around 1-2%, λ_{ice} is required to be considerably larger than λ_{mantle} for all physical values of $\mathcal{C}_1$. This indicates that approximations of the viscosity constant using inferences from mantle rocks may not be as accurate as previously supposed.

Reverting back to our original boundary conditions, we now wish to instead prescribe a constant compaction stress $\tilde{\sigma}_{zz} = -\sigma$ acting on the ice-water mixture from above, and a constant shear stress $\tilde{\sigma}_{xz} = \tau$ acting horizontally across the top surface. Dimensionally, in

the small $\mathcal{R}$ limit, we had obtained

$$\sigma = \frac{\xi \mathcal{W}}{H_0}, \tag{5.25}$$

and from §4.1, the shear stress may be expressed simply as

$$\tau = \frac{\eta \mathcal{U}}{H_0}. \tag{5.26}$$

Using equations (**??**) & (**??**), we may now recast the dimensional porosity time-evolution equation in terms of the imposed shear and normal stresses, by substituting them into (**??**) to obtain

$$\dot{\varphi} = \frac{\sigma^2}{\mathcal{L}\xi\rho} + \frac{\tau^2}{\mathcal{L}\eta\rho} - \frac{\sigma}{\xi}(1-\varphi). \tag{5.27}$$

Expanding in φ, we then have

$$\dot{\varphi} = \frac{\sigma^2}{\mathcal{L}\xi_0\rho} e^{\lambda(\varphi-\varphi_0)} \left(\frac{\varphi}{\varphi_0}\right) + \frac{\tau^2}{\mathcal{L}\eta_0\rho} e^{\lambda(\varphi-\varphi_0)} - \frac{\sigma}{\xi_0} e^{\lambda(\varphi-\varphi_0)}(1-\varphi)\left(\frac{\varphi}{\varphi_0}\right). \tag{5.28}$$

Then, rescaling time as $\hat{t} = \xi_0 t \varphi_0 e^{\lambda\varphi_0}/\sigma$ and dropping the hat gives us a dimensionless porosity evolution equation

$$\dot{\varphi} = \mathcal{D}_1 e^{\lambda\varphi}\varphi + \mathcal{D}_2 e^{\lambda\varphi} - e^{\lambda\varphi}(1-\varphi)\varphi, \tag{5.29}$$

where $\mathcal{D}_1 = \sigma/\mathcal{L}\rho$ and $\mathcal{D}_2 = \xi_0\tau^2/\mathcal{L}\eta_0\rho\sigma\varphi_0$. We are now looking to obtain the steady state solutions given constant applied stresses, and so we set the right hand side of (**??**) equal to 0, yielding

$$\varphi_e^2 + (\mathcal{D}_1 - 1)\varphi_e + \mathcal{D}_2 = 0, \tag{5.30}$$

a quadratic equation with two roots: stable and unstable steady-state solutions. The experiment is set up to impose normal stresses of approximately 250 kPa and shear stresses of approximately 200 kPa [Zoet & Iverson (2015)], and these typical values lead to $\mathcal{D}_1 = 0.81, \mathcal{D}_2 = 52$. Note that with these constant stress boundary conditions the steady state solutions are now independent of the viscosity constant λ. These proposed experimental values yield complex solutions of equation (**??**) however, and so here the model predicts that no steady states exists. As before, a decrease in prescribed strain rates reme-

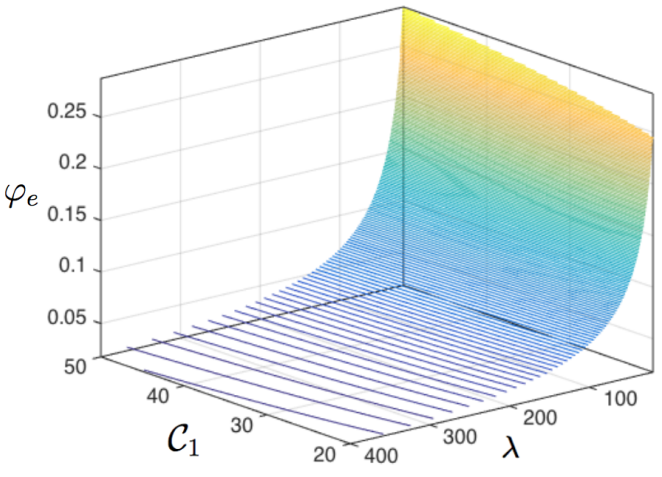


Figure 5.5: Contours represent level contours of φ_e.

dies the problem, yielding real solutions. Upon considering a reduction in the horizontal shear stress component $\tilde{\sigma}_{xz}$, for example, down to just 2 kPa, a stable steady-state solution emerges at $\varphi_e \approx 0.02$, a typical liquid water fraction that we might expect to find in an experiment mimicking regions of temperate ice. In a similar vein to before, we may well be concerned that stresses of this magnitude could result in such minor deformation that the time-scales involved may simply be too large for this setup to be experimentally viable, at least according to the present reduced model.

5.5 Large-scale Applications

Based on the model equations, we're also able to provide some estimates for the melt rate and subsequent drainage from temperate zones at the base of ice stream margins. In Chapter 4, the total drainage $\mathfrak{D}$ is equal to the mass flux of liquid water through the ice base, which we can approximate as $\rho_f w_f \mathcal{A}$ for the experiment or $\int_{\mathcal{A}} \rho_f w_f dA$ for a temperate glacier, where A is the area of the temperate zone in contact with the base. Re-dimensionalising equation (**??**) and expressing the melt rate as a function of the stresses τ and σ allows us to calculate the melt rate in the small $\mathcal{R}$ limit:

$$\Gamma = \frac{\sigma^2}{\mathcal{L}\xi} + \frac{\tau^2}{\mathcal{L}\eta}. \tag{5.31}$$

The quadratic dependence of the melt rate on the stresses highlights the importance of the effects of viscous dissipation in temperate ice. It also shows that in areas where shear stresses are particularly high compared to the overburden pressure, such as in fast shallow flows, shearing dominates the melting process since η is much less than ξ.

Given a porosity of around 1%, $\mathcal{L}$ as suggested in Table 3.1 and typical stresses present in an ice stream margin: $\tau = 100$ kPa, $\sigma = 1$ MPa, we obtain a melt rate of $\Gamma = 3.0 \times 10^{-9}$ kg m^{-3} s^{-1}. $\mathfrak{D}$ will then be given by the integral of Γ over the region enclosed by the CTS, which we will denote Ω:

$$\mathfrak{D} = \int_{\Omega} \Gamma dV. \tag{5.32}$$

For simplicity, we assume both uniform porosity and uniform stress distributions throughout the volume, whilst conceding that this makes our estimate on the total drainage due to englacial melting very approximate since τ and φ may vary strongly between the base and the top of Ω. Using predictions from Suckale et al. (2014) on the cross sectional area of the temperate zone that lies below Dragon Margin, equation (**??**) gives us a drainage of $\mathfrak{D} = 36$ m^3 yr^{-1} per metre downstream due to englacial melting. This is very similar to the drainage predicted here in both Suckale et al. (2014), at between 25 and 26.5 m^3 yr^{-1} per metre, and Perol et al. (2015), at between 36 and 47 m^3 yr^{-1} per metre. Our value of 36 m^3 yr^{-1}, however, should be an underestimate of the true melt rate, since unlike the other two models ours does not include additional melting at the ice-bed interface.

We can also use the melt rate to predict the total amount of local ice thinning due to englacial melting by multiplying Γ by the ice thickness. Taking the average depth of the temperate zone

to be around 100m, we predict that englacial melting should decrease ice thickness at a rate of around 9 m yr^{-1}. Since the rate of average snow accumulation is typically taken to be around 0.1 m yr^{-1} across the ice sheet and the compaction velocity $\mathcal{W}$ was first taken to be around 30 mm yr^{-1}, this figure does sound rather large by comparison. We should, however, remember that this thinning is highly localised at the ice stream margins, where large surface depressions and even chaotic crevassing can be observed in some cases. The value provided is also a very rough estimate, and we suggest that it is treated as such.

According to this reduced theory of two-phase flows, stable steady-state solutions for the porosity can be achieved when assuming the compaction length δ to be much larger than the height of the chamber H. In order to progress, the level of sophistication of the model should be questioned and revised. Here the weight of the ice was taken to be negligible when compared to the compaction stresses, though an introduction of a gravitational driving stress would be likely to further strengthen the flow, increasing the melt rate. The densities ρ_m and ρ_f were taken to be equal in this model, but in fact we know that $\rho_m < \rho_f$. Including this leads to a density-driven downward flow of the liquid phase, increasing the rate at which water is supplied to the base, affecting the dynamics. As an initial condition, the porosity was also assumed to be set as uniform. In a controlled experiment, this is certainly achievable, but isn't always the case for glaciers, where pockets of water may accumulate within the fabric of the ice and the porosity may be highly non-uniform. An improved model should account for this.

In lifting these few key assumptions, the model equations can no longer be reduced and decoupled into simple sets of ODEs which can be solved individually, and often analytically. In going forward we should look to employ numerical techniques on the full set of coupled PDEs, an idea discussed briefly in the next chapter and proposed as part of a future research plan for those interested in taking this work forward.

Chapter 6

Discussion & Conclusions

In Chapters 1 and 2 we argued that new glaciological models are needed in order to better capture the dynamic effects in regions of temperate ice, such as those that are inferred to exist in the vicinity of ice stream margins. In particular, we built upon the works of McKenzie (1984), Aschwanden et al. (2012) and Suckale et al. (2014), introducing a two-phase fluid dynamical framework for coupled ice-water mixtures in an attempt to describe the physics within these zones.

The full 1-dimensional model was then introduced and derived in Chapter 3, complemented by a set of constitutive laws based on findings from both theoretical and experimental glaciology, as well as from progress made in the field of magma-mantle dynamics. Intending to make our model findings experimentally verifiable, we proposed using apparatus adapted from Iverson & Peterson (2011), matching our initial and boundary conditions to this setup. This could then be used to draw inferences on the texture and rheology of ice, as well as make predictions for larger-scale glacier behaviour.

In Chapter 4, we introduced a reduced version of the model, and specifically investigated a Filter Press compaction problem, focussing on the instantaneous response of the pressure and ice velocity profiles to vertical and horizontal stresses applied to the top of the ice-water column. In the limit of infinite compaction length, ice velocity was shown to decrease linearly with depth and compaction effects were therefore shown to be uniform throughout the domain.

In Chapter 5, we showed that in this infinite compaction length limit, assuming a constant permeability, constant shear viscosity and constant compaction viscosity led to an exponential decay in the chamber height to zero under an applied vertical stress. Upon allowing these parameters to vary with porosity, according to the constitutive laws introduced in Chapter 3, the model was revised to account for the subsequent increase in viscosity as a result of diminishing porosity. Hereafter the chamber height reduced asymptotically to a non-zero value according to mass conservation, where the effects of melting were neglected.

We then went on to show that constant horizontal shearing of the ice-water mixture from above gives rise to a Couette flow where viscous dissipation drives a logarithmically increasing porosity in time. Combining horizontal and vertical stresses with drainage led to the conclusion that given the right experimental conditions, these processes could be balanced to produce steady-state solutions where we could retain a constant liquid volume fraction within the cham-

ber. If the stable steady-state solution is to have a porosity of around 2%, as has been observed in temperate ice, the model suggests that this requires a much larger viscosity constant λ than was assumed from the analogy with mantle rocks. That is, we predict that the viscosity of glacier ice is much more sensitive to changes in porosity than that of the mantle. In addition, stresses were typically required to be much smaller than had originally been assumed by the experimental setup, suggesting that very low strain rates are needed in order to achieve a stable steady-state solution for the porosity. Finally, we presented an estimate for the total amount of meltwater drainage from Dragon Margin: $\mathfrak{D} = 36$ m^3 yr^{-1} per metre downstream which was reasonably consistent with existing estimates.

Since the model was originally set up with the intention to better capture dynamic effects in regions of temperate ice, we might ask what insight does any of this give us about what could be going on in an ice stream margin? This model suggests that under the right conditions, given the assumption of thermal equilibrium, the presence of meltwater and observed drainage can be maintained purely by a combination of compaction, melting and viscous dissipation. In addition, these contributions can "balance out", leading to a sustained constant liquid water fraction within the temperate zone. Of course, the ice geometry is considerably more complex in reality, and the approximation of simple shear considered here is unlikely to hold accurately throughout the ice stream. In turn this will mean that the water and ice flow velocities will likely be more complicated than predicted in this report.

Since the overburden pressure induced at an ice stream margin leads to compaction of the ice matrix, and the large strain rates induced by the ice stream's flow relative to the stagnant ice ridge leads to large amounts of viscous dissipation, we argue that the experimental results would act as a strong indicator of ice-stream margin dynamics. And though we acknowledge there is still much work to be done in terms of advancing the model, we are confident that these findings readily apply to ice stream margins, and may eventually shed light on the conditions required for their onset, stability and migration.

6.1 Recommendations for Experimentalists

According to the McKenzie equations, it's possible to retain stable levels of meltwater using the setup detailed in Chapter 3, and so first of all we would recommend experimental work that could either support or contradict this finding. These results imply, however, that the strain rates needed to produce such stable levels of meltwater would be so small that the timescale for appreciable levels of deformation may be too large, at least for any viable experiment. They are such that not only could the process become far too consumptive in terms of energy and time, but that other factors affecting ice deformation could become increasingly important over the course of the experiment. Rheological factors may be of particular concern, though little research has been done into this sub-field in glaciology. To this end, we would recommend that experimental work be done in order to more accurately ascertain the viscosity constant λ for glacier ice.

In assuming that the average grain size would be roughly 1 to 10mm in size, treating ice as a continuum on glacial length-scales seems very reasonable, though on the scale of an experiment,

this may not be such a good supposition. In order to create a representative volume element for the ice-water mixture, its size may only be an order of magnitude less than that of the entire domain. We recommend that these kinds of experiments be carried out for this very reason - to investigate grain-scale effects - since they seem unlikely to be negligible. We stress that such an experiment as this is scientifically useful only in that it attempts to mimic glacial conditions, and so it's important that the model equations can be applied equally on both scales.

A further scaling problem arises in the assumption of an "infinite compaction length", certainly a reasonable approximation for the experiment but potentially a poor approximation for an ice stream margin, which is typically hundreds of metres in depth. We should expect that an investigation of the full time-dependent problem for "finite compaction lengths" would improve consistency between the experiment and the temperate ice regions themselves.

6.2 Advancing the Two-Phase Model

Investigating the finite compaction length problem amounts to considering the full non-dimensionalised model equations (**??**) – (**??**) and evaluating these six coupled PDEs in a 1D numerical model. We can avoid the complications of solving a moving boundary problem by introducing a coordinate transformation from (z,t) to $(\mathcal{Z},\tau)$, converting this to a fixed boundary problem. This can be achieved by using the prescription $z = \mathcal{Z}H(t)/H_0$ so that the domain $z \in [0, H(t)/H_0]$ corresponds to $\mathcal{Z} \in [0,1]$. The derivatives $\partial/\partial z$ and $\partial/\partial t$ then transform according to relations (**??**) and (**??**):

$$\frac{\partial}{\partial z} = \frac{H_0}{H}\frac{\partial}{\partial \mathcal{Z}}, \tag{6.1}$$

$$\frac{\partial}{\partial t} = \frac{\partial}{\partial \tau} - \frac{\mathcal{Z}\dot{H}}{H}\frac{\partial}{\partial \mathcal{Z}}. \tag{6.2}$$

The application of the coordinate and derivative transformations to equations (**??**) – (**??**) and the corresponding boundary conditions results in a fixed boundary problem which can be solved numerically.

Without the requirement of an "infinite compaction length", it may turn out that the experiment's horizontal and vertical strain rates needn't be so small, and that the time needed to run the experiment is much shorter than has been inferred in the infinite compaction length limit. Otherwise, we may still face the problem that the continuum assumption is too strong for the experimental scales involved, or that the equations themselves may need some revision in order to better fit with observation. Regardless, finding the solutions of the full 1D numerical problem is the natural next step in this line of work.

6.3 Recommendations for Theoreticians & Future Work

Energy conservation of multi-phase flows may be recast in terms of a statement of conservation of specific enthalpy, where we have generalised from the isochoric (bulk incompressibility) conventions of the current model. The present is an opportune time to develop this

formulation into an enthalpy method since recent advances in two-phase modelling of coupled magma-mantle dynamics have introduced methods from metallurgy into geophysical calculations; imposing conservation of enthalpy in a multi-phase system [Katz (2008)]. More recent efforts have also utilised such techniques in polythermal glaciology [Aschwanden et al. (2012)], but have not yet been generalised to two-phase ice-water flows.

The current setup could be expanded further by including a subglacial hydrological component, accounting for the meltwater drainage at the permeable interface. In coupling this hydrology to the till, this could also lay the foundations for more advanced models that incorporate hydrologically controlled erosion and sediment motion, for example.

It should also be noted that the self-consistent physics of these ice streams is not included in large-scale ice sheet models [Payne & Dongelmans (1997), Bougamont et al. (2011), van Pelt & Oerlemans (2012)]. It is this very shortcoming that motivates the development of small-scale models such as the one constructed in this report. In utilising the fully resolved dynamics on a local scale, the current model can then be used as an essential foundation in constructing upscaling parameterisations. Such upscaling could enable ice stream dynamics to be accurately resolved in large-scale models, enhancing their current predictive capabilities. There is still some way to go in extending the current model before this is possible, however.

The development of small-scale glaciological models of ice streams allows us to tackle fundamental questions such as how do these streams emerge and evolve? What sets their characteristic scales such as size and flow velocity? And how might these change in the future? Upscaling to a large-scale model, however, allows us to ask bigger and more globally relevant questions such as what is the total rate and volumetric extent of melting in the Antarctic? What is the corresponding sea-level rise? And what are the consequent effects on the climate? We remain confident that better answers to these questions will emerge from the ongoing interplay between observation, experiment, theory, and simulation.

It is the theoretical work and the accompanying simulations that we believe will prove to be most essential in creating and analysing a mathematical formulation by which we may test our hypotheses; allowing us to disentangle the roles of different physical mechanisms in controlling the spatial and temporal variability of ice streams. It is important that these advances continue to shed light on the coupling of ice-stream dynamics to the cryosphere, for reasons both scientific and political, since better information should inevitably result in better action.

Bibliography

[1] Aschwanden A, Bueler E, Kroulev C, Blatter H, 2012, An enthalpy formulation for glaciers and ice sheets, *Journal of Glaciology* **58**, No. 209, 441-457(17).

[2] Bamber JL, 2000, Widespread complex flow in the interior of the Antarctic ice sheet, *Science* **287**, 1248-1250.

[3] Bamber JL, Riva REM, Vermeersen BLA, LeBrocq AM, 2009, Reassessment of the Potential Sea-Level Rise from a Collapse of the West Antarctic Ice Sheet, *Science* **324**, No. 901.

[4] Beem L, Jezek K, Van der Veen C, 2010, Basal melt rates beneath Whillans Ice Stream, West Antarctica, *Journal of Glaciology* **56**, No. 19, 647-654.

[5] Bell RE, Creyts TT, Braaten D, Corr HFJ, Das I, Damaske D, Frearson N, Jordan T, Rose K, Studinger M, Wolovick M, 2011, Widespread persistent thickening of the East Antarctic Ice Sheet by freezing from the base, *Science* **331**, No. 6024, 1592-1595.

[6] Bindschadler R, Vornberger P, 1998, Changes in the West Antarctic ice sheet since 1963 from declassified satellite photography, *Science* **279**, No. 5351, 689-692.

[7] Bougamont M, Christoffersen P, Hubbard AL, Fitzpatrick AA, Doyle SH, Carter SP, 2011, Sensitive response of the Greenland Ice Sheet to surface melt drainage over a soft bed, *J. Geophys. Res.* **116**.

[8] Christoffersen P, 2003, Thermodynamics of Basal Freeze-On: Subglacial property changes and ice sheet response, *Department of Civil Engineering, Technical University of Denmark*, Ph.D. Thesis.

[9] Clarke TS, Liu C, Lord NE, Bentley CR, 2000, Evidence for a recently abandoned shear margin adjacent to ice stream B2, Antarctica, from ice-penetrating radar measurements, *J. Geophys. Res.* **105**, B6.

[10] Cuffey KM, Paterson WSB, 1969, The Physics of Glaciers, 1st ed., *Butterworth Heinemann.*

[11] Cuffey KM, Paterson WSB, 2010, The Physics of Glaciers, 4th ed., *Butterworth Heinemann.*

[12] Duval P, 1977, The role of the water content on the creep rate of polycrystalline ice, *IAHS-AISH, Proceedings of the Grenoble Symposium*, No. 118.

[13] Echelmeyer K, Harrison W, 1999, Ongoing margin migration of ice stream B, Antarctica, *Journal of Glaciology* **45**, 361-369.

[14] Echelmeyer K, Harrison W, Larsen C, Mitchell J, 1994, The role of the margins in the dynamics of an active ice stream, *Journal of Glaciology* **40**, No. 136, 527-538.

[15] Fahnestock M, Scambos T, Bindschadler R, Kvaran G, 2000, A millennium of variable ice flow recorded by the Ross ice shelf, Antarctica, *Journal of Glaciology* **46**, No. 155, 652-664.

[16] Fowler A, 2013, Chapter 10: Glaciers & Ice Sheets.

[17] Fowler AC, 1984, On the transport of moisture in polythermal glaciers, *Geophys. Astrophys. Fluid Dynamics* **28**, 99-140.

[18] Glasser NF, 2011, Polythermal glaciers, *Springer Netherlands*, 865-867.

[19] Greve R, 1997, A continuum-mechanical formulation for shallow polythermal ice sheets, *Philosophical Transactions of the Royal Society A* **355**, No. 1726.

[20] Harrison W, Echelmeyer KA, Larsen C, 1998, Measurement of temperature in a margin of Ice Stream B, Antarctica: Implications for margin migration and lateral drag, *Journal of Glaciology* **44** No. 148.

[21] Hutter K, 1982, A mathematical model of polythermal glacier and ice sheets, *Geophys. Astrophys. Fluid Dynamics* **21**, 201-224.

[22] Ince EL, 1956, Ordinary Differential Equations, *New York: Dover Publications*.

[23] Iverson NR, Petersen BB, 2011, A new laboratory device for study of subglacial processes: first results on ice-bed separation during sliding, *Journal of Glaciology* **57**, No. 206, 1135-1146.

[24] Jacobel R, Scambos T, Nereson N, Raymond C, 2000, Changes in the margin of ice stream C, Antarctica, *Journal of Glaciology* **46**, No. 152, 102-110.

[25] Jacobel R, Scambos T, Raymond C, Gades A, 1996, Changes in the configuration of ice stream flow from the West Antarctic ice sheet, *J. Geophys. Res.* **101**, B3, 5499-5504.

[26] Jacobson HP, Raymond CF, 1998, Thermal effects on the location of ice stream margins, *J. Geophys. Res.* **103**, B6, 12111-12122.

[27] Joughin I, MacAyeal DR, Tulaczyk S, 2004, Basal shear stress of the Ross ice streams from control method inversions, J. Geophys. Res. **109**, B9.

[28] Katz RF, 2008, Magma Dynamics with the Enthalpy Method: Benchmark Solutions and Magmatic Focusing at Mid-ocean Ridges, *J. Petrol.* **49**, No. 12, 2099-2121.

[29] Katz RF, 2015, An Introduction to Coupled Magma/Mantle Dynamics.

[30] Kyrke-Smith TM, Katz RF, Fowler AC, 2014, Subglacial hydrology and the formation of ice streams, *Proc. R. Soc. A* **470**.

[31] Lliboutry L, Duval P, 1985, Various isotropic and anisotropic ices found in glaciers and polar ice caps and their corresponding rheologies, *Ann. Geophys.* **3**, No. 2, 207-224.

[32] McKenzie D, 1984, The generation and compaction of partially molten rock, *J. Petrol.* **25**, No. 3, 713-765.

[33] Miller KJ, Zhu W, Montési LGJ, Gaetani GA, 2013, Experimental Quantification of Permeability of Partially Molten Mantle Rock, *Earth and Planetary Science Letters.*

[34] Nye JF, Frank FC, 1973, Hydrology of the Intergranular Veins in a Temperate Glacier, H. H. Wills Physics Laboratory, University of Bristol, Bristol, England.

[35] Payne AJ, Dongelmans PW, 1997, Self-organization in the thermomechanical flow of ice sheets *J. Geophys. Res.* **102**.

[36] Payne AJ, Huybrechts P, Abe-Ouchi A, Calov R, Fastook JL, Greve R, Marshall SJ, Marsiat I, Ritz C, Tarasov L, Thomassen MP, 2000, Results from the EISMINT model intercomparison: the effects of thermomechanical coupling, *Journal of Glaciology* **46**, No. 153, 227-238.

[37] Perol T, Rice JR, 2011, Control of the width of West Antarctic ice streams by internal melting in the ice sheet near the margins, abstract C11B-0677 presented at 2011 Fall Meeting, AGU, San Francisco, Calif.

[38] Perol T, Rice JR, 2015, Shear Heating and Weakening of the Margins of West Antarctic Ice Streams, *Geophys. Res. Lett.*

[39] Perol T, Rice JR, Platt JD, Suckale J, 2015, Subglacial Hydrology and Ice Stream Margin Locations, *J. Geophys. Res. Earth Surf.*

[40] Perrot P, 1998, A to Z of Thermodynamics, *Oxford University Press.*

[41] Piazolo S, Wilson CJL, Luzin V, Brouzet C, Peternell M, 2013, Dynamics of ice mass deformation: Linking processes to rheology, texture, and microstructure, *Geochemistry, Geophysics, Geosystems* **14**, No.10, 4185-4194.

[42] Price SF, Conway H, Waddington ED, Bindschadler RA, 2008, Model investigations of inland migration of fast-flowing outlet glaciers and ice streams, *Journal of Glaciology* **54**, No. 184, 49-60.

[43] Rignot E, Mouginot J, Scheuchl B, 2011, Ice flow of the Antarctic ice sheet, *Science* **333**, 1427-1430.

[44] Rudge JF, Bercovici D, Spiegelman M, 2011, Disequilibrium Melting of a Two Phase Multicomponent Mantle, *Geophys. J. Int.* **184**, 699-718.

[45] Schoof C, 2004, On the mechanics of ice-stream shear margins, *Journal of Glaciology* **50**, No. 169, 208-218.

[46] Schoof C, 2010, Ice-sheet acceleration driven by melt supply variability, *Nature* **468**, No. 325, 803-806.

[47] Schoof C, 2012, Thermally driven migration of ice-stream shear margins, *J. Fluid Mech.* **712**, 552-578.

[48] Schoof C, Hewitt IJ, 2013, Ice-Sheet Dynamics, *Annual Reviews of Fluid Mechanics* **45**, 217-239.

[49] Shabtaie S, Bentley C, 1988, Ice-thickness map of the West Antarctic ice streams by radar sounding, Ann. Glaciol. **11**, 126-136.

[50] Shabtaie S, Bentley CR, 1987, West Antarctic ice streams draining into the Ross Ice Shelf: Configuration and mass balance, *J. Geophys. Res.* **92**.

[51] Simpson G, Spiegelman M, Weinstein M, 2010, A Multiscale Model of Partial Melts: 2. Numerical Results, *J. Geophys. Res.* **115**.

[52] Stokes CR, Clark CD, 2001, Palaeo-ice streams, *Quaternary Science Reviews* **20**, No. 13, 1437-1457.

[53] Suckale J, Platt JD, Perol T, Rice JR, 2014, Deformation-induced melting in the margins of the West Antarctic ice streams, *J. Geophys. Res. Earth Surf.* **19**, 1004-1025.

[54] Van Pelt WJJ, Oerlemans J, 2012, Numerical simulations of cyclic behaviour in the Parallel Ice Sheet Model (PISM), *Journal of Glaciology* **58**, 347-360.

[55] Vaughan DG, Corr HFJ, Fausto F, Frearson N, O'Hare A, Mach D, Holt JW, Blankenship DD, Morse DL, Young DA, 2006, New boundary conditions for the West Antarctic ice sheet: Subglacial topography beneath Pine Island Glacier, *Geophys. Res. Lett.* **33**.

[56] Vaughan DG, Spouge JR, 2002, Risk Estimation of Collapse of the West Antarctic Ice Sheet, *Springer Climatic Change* **52**, 65-91.

[57] Vogel SW, Tulaczyk S, Kamb B, Engelhardt H, Carsey FD, Behar AE, Lane AL, Joughin I, 2005, Subglacial conditions during and after stoppage of an Antarctic Ice Stream: Is reactivation imminent?, *Geophys. Res. Lett.* **32**.

[58] Weast RC, 1981, CRC Handbook of Chemistry and Physics 62nd edition.

[59] Whillans I, Van Der Veen C, 1993, New and improved determinations of velocity of Ice Streams B and C, West Antarctica, *Journal of Glaciology.*

[60] Zhu W, Gaetani GA, Fusseis F, Montési LGJ, De Carlo F, 2011, Microtomography of Partially Molten Rocks: Three-Dimensional Melt Distribution in Mantle Peridotite, *Science* **332**, 88-90.

[61] Zoet LK, Iverson NR, 2015, Experimental determination of a double-valued drag relationship for glacier sliding, *Journal of Glaciology* **61**, No. 225.

[62] Zotikov I, 1986, The Thermophysics Of Glaciers, D. Reidel, Mass.